Investigation of Power Grid Islanding Based on Nonlinear Koopman Modes

Johan Fredrik Raak

KTH Electrical Engineering

Degree project in
Electric Power Systems
Second Level,
Stockholm, Sweden 2013

XR-EE-EPS 2013:001

KTH Electrical Engineering

Investigation of Power Grid Islanding Based on Nonlinear Koopman Modes

JOHAN FREDRIK RAAK

Master of Science Thesis in Electric Power Systems
at the School of Electrical Engineering
Royal Institute of Technology
Stockholm, Sweden, September 2013
Supervisors: Harold R. Chamorro (KTH) and Takashi Hikihara (Kyoto University)
Examiner: Mehrdad Ghandhari

XR-EE-EPS 2013:001

Abstract

To view the electricity supply in our society as just sockets mounted in our walls with a constant voltage output is far from the truth. In reality, the power system supplying the electricity or *the grid*, is the most complex man-made dynamical system there is. It demands severe control and safety measures to ensure a reliable supply of electric power. Throughout the world, incidents of widespread power grid failures have been continuously reported. The state where electricity delivery to customers is terminated by a disturbance is called a blackout. From a state of seemingly stable operating conditions, the grid can fast derail into an uncontrollable state due to cascading failures. Transmission lines become automatically disconnected due to power flow redirections and parts of the grid become isolated and *islands* are formed. An islanded sub-grid incapable of maintaining safe operation conditions experiences a blackout. A widespread blackout is a rare, but an extremely costly and hazardous event for society.

During recent years, many methods to prevent these kinds of events have been suggested. *Controlled islanding* has been a commonly suggested strategy to save the entire grid or parts of the grid from a blackout. Controlled islanding is a strategy of emergency control of a power grid, in which the grid is intentionally split into a set of islanded subgrids for avoiding an entire collapse. The key point in the strategy is to determine appropriate separation boundaries, i.e. the set of transmission lines separating the grid into two or more isolated parts.

The power grid exhibits highly nonlinear response in the case of large failures. Therefore, this thesis proposes a new controlled islanding method for power grids based on the nonlinear Koopman Mode Analysis (KMA). The KMA is a new analyzing technique of nonlinear dynamics based on the so-called Koopman operator. Based on sampled data following a disturbance, KMA is used to identify suitable partitions of the grid.

The KMA-based islanding method is numerically investigated with two well-known test systems proposed by the Institute of Electrical and Electronics Engineers (IEEE). By simulations of controlled islanding in the test system, it is demonstrated that the grid's response following a fault can be improved with the proposed method.

The proposed method is compared to a method of partitioning power grids based on spectral graph theory which captures the structural properties of a network. It is shown that the intrinsic structural properties of a grid characterized by spectral graph theory are also captured by the KMA. This is shown both by numerical simulations and a theoretical analysis.

Keywords: Controlled islanding, grid partitioning, power system monitoring, Koopman mode analysis, spectral graph theory.

Referat

Att betrakta elförsörjningen som endast någonting konstant som vi matas med via våra uttag i hemmet är långt ifrån hela sanningen. Elkraftsystemet som försörjer samhället med elektricitet betraktas som ett av de mest avancerade och komplexa dynamiska systemen som skapats av människor. Med jämna mellanrum har fall av stora elnätskollapser rapporterats från olika delar av världen. Tillståndet när strömförsörjningen till kunderna i systemet stängs av kallas ett elavbrott eller en *blackout*. Från ett till synes stabilt tillstånd i systemet, kan tillståndet snabbt försämras och fel kan propagera på ett lavinartat sätt och äventyra stabila driftvillkor. Transmissionsledningar kan överbelastas på grund av ett förändrat kraftflöde och kopplas bort automatiskt av säkerhetsreläer. På deta sätt kan delar av systemet blir bortkopplade och subsystem eller isolerade öar i systemet bildas. Om dessa isolerade öar inte kan bibehålla stabila driftvillkor kommer det att inträffa ett elavbrott.

Under det senaste decenniet har många olika strategier föreslagits för att förhindra utbredda elavbrott. *Controlled islanding* (kontrollerad splittring) är en populärt föreslagen strategi för att rädda hela eller delar av systemet från en kollaps. Det är en typ av nödåtgärd som används för att på ett kontrollerat sätt splittra systemet för att begränsa risken för propagering av fel som leder till omfattande elavbrott. Huvudproblemet är att bestämma lämpliga separationspunkter för att erhålla bästa utfall, d.v.s. att bestämma vilka transmissionledningar som mest lämpligast bör kopplas bort.

Ett elkraftsystem uppvisar mycket ickelinjärt beteende som respons av en stor störning. På grund av detta föreslår denna uppsats en ny metod för splittring av ett elkraftsystem baserat på Koopman Mode Analysis (KMA) som är en analysmetod av ickelinjära system och är baserad på så kallade Koopman operatorn. Baserat på sampel av data från ett dynamiskt skeende i systemet identifieras lämpliga separationspunkter.

Metoden utvärderas numeriskt genom simuleringar av två välkända testsystem föreslagna av *Institute of Electrical and Electronics Engineers* (IEEE). Genom kontrollerad splittring demonstreras det att responsen till följd av ett fel kan förbättras.

Den föreslagna metoden jämförs med en metod baserad på grafteori för att partitionera nätverk. Grafteori fångar de strukturella egenskaperna hos ett nätverk. Resultatet i den här uppsatsen visar att den KMA-baserade metoden som analyserar dynamiken i elnätet, även kan fånga de strukturella egenskaperna från grafteori. Detta resultat visas både experimentellt och diskuteras utifrån en teoretisk analys.

Acknowledgment

First and foremost I want to thank Kyoto University and especially Professor Takashi Hikihara who agreed with my one year stay in Kyoto. The one year stay in Japan gave me valuable lessons and experiences for my future life and career.

I also want to thank Yoshihiko Susuki for his support, suggestions, discussions and patience. More than that, I want to thank all the helpful and nice people at the Hikihara laboratory.

Lastly, I am thankful to my supervisor at the Royal Institute of Technology (KTH), Harold Chamorro who agreed to supervise me in such a great way, and examiner Mehrdad Ghandhari who accepted the master thesis proposal.

Contents

Contents

Chapter 1

Introduction

1.1 Background

Large scale power systems or *power grids* are the largest and most complex dynamical systems created by humans. Simplistically, the grid constitutes of transmission lines at different voltage levels connected by substations, power suppliers and costumers. The power generation incorporates technically advanced generation sources such as nuclear power plants as well as many renewable and stochastically varying sources like solar and wind power. The bare size of the physically interconnected network spans over vast countries and even across borders. The operation of the system demands severe monitoring and control measures.

In recent years, the power grids are generally operated closer to their maximum capabilities due to increasing power demands in combination with environmental policies. In order to meet the increasing demands as well as enabling the introduction of the renewable energy sources, advanced power electronic control systems are increasingly being installed. Moreover, information and communication technologies are integrated for a smart control and monitoring of the system. In other words, the complexity as well as the vulnerability have increased.

A power grid exhibits highly nonlinear response in the case of extensive failures [1]. Cascading failures initiated by a severe disturbance in large-scale power grids have been repeatedly reported all over the world from countries such as North America, Sweden, Italy and India [2–4]. The state where electricity delivery to customers is terminated by a disturbance is called a blackout. From a state of seemingly stable operating conditions, the system can fast derail into an uncontrollable state due to cascading failures propagating in the system. Overloaded transmission lines are automatically disconnected due to redirection of power flow in the system and parts of the system can become isolated and *islands* are formed. An islanded subsystem incapable of maintaining safe operating conditions experiences a blackout. A widespread blackout is a rare but an extremely costly and hazardous event for the modern society.

Monitoring and coordinated control are of vital importance for maintaining the

electricity supply and avoid large scale failures [2]. As one of the effective coordinated controls, the so-called controlled islanding strategy has been studied recently. It is a strategy of emergency control of a power grid, in which the grid is intentionally split into a set of isolated sub-grids in case of large failures in an attempt to avoid a widespread blackout.

1.2 Problem Definition and Objective

The purpose of this thesis is to investigate a new controlled islanding strategy based on nonlinear dynamical systems and to investigate its performance by simulations of standard benchmark systems. The aim is to prevent a total blackout using the proposed method. Cascading failures and associated dynamics are highly complicated and need to be analyzed and controlled from a viewpoint of nonlinear dynamical systems. The so-called Koopman Mode Analysis (KMA) is a new technique of nonlinear modal decomposition based on the Koopman operator [5, 6]. Recently, the theory has been applied to power system analysis [7–9].

In this thesis, the KMA is applied on measurements of generator frequencies and bus voltage angles. Based on the KMA on bus voltage angles, the test system is split into isolated sub-systems. To maintain a safe operation for each constructed island, a balance between load and generation in the island needs to be considered.

The test system is simulated with the power simulation toolbox PSAT [10]. The proposed islanding method is evaluated by applying critical disturbances.
In short, the goal is set as follows:

> **Goal**. A fully functional islanding strategy using the Koopman Mode Analysis is implemented and proven to be successful in avoiding a blackout (instability) for critical disturbances. This will be demonstrated on at least one test system. The results of the proposed islanding strategy will be compared to results obtained from at least one other islanding method.

1.3 Thesis Overview

The remainder of this thesis is organized as follows. In chapter 2, background and mechanisms of cascading failures in power grids are given and common prevention methods are described. In chapter 3 the theoretical descriptions of KMA as well as spectral graph theory are given. The proposed islanding method based on the KMA is presented in chapter 4. In chapter 5 simulations are performed and numerical results are discussed. Lastly, a summary, conclusions and suggestions for future studies are given in chapter 6. The mathematical description for the power system simulations are given in appendix A. During the lapse of this project, one technical report and one conference paper were produced and both are briefly described in appendix C.

Chapter 2

Controlled Islanding

A power grid is continuously subjected to small and large disturbances which do not threaten a safe operation of the grid. Load fluctuations and variations in the power generation are examples of small disturbances. Disconnection of important transmission lines or loss of large power plants are common cases of large disturbances. For example, transmission lines are occasionally short-circuited as a consequence of falling trees or infrastructural damage caused by extreme weather conditions.

In recent years, as a consequence of the continuous increase of renewable energy sources, generation becomes more stochastic compared to the case where conventional power sources such as nuclear, hydro, coal and gas are mainly used. An increasing demand of control, power electronics and IT infrastructure are demanded to enable this increase and ensure safe operation. Also, the power grid is more often operated closer to its operation limit. In this way, the grid has both become more vulnerable and its behavior more complex.

Only on rare occasions, a widespread blackout occurs, however local blackouts occur frequently [1]. Famous blackouts during recent years have occurred in North America, Sweden, Italy, Russia and India [2–4, 11]. To some extent, it is inevitable that the grid sooner or later will experience a large-scale blackout [12]. However, sophisticated prevention strategies and control measures can minimize the occurrence. Improved monitoring that enables coordination and control of large scale power grids is generally considered as an important counter-measures [2]. A Wide Area Measurement System (WAMS) provides measurements via Phasor Measurement Units (PMUs) [13]. PMU devices are able to measure desired quantities such as voltage or currents at a high sampling frequency, coordinated in time by GPS measurements.

There are numerous factors contributing to the vulnerability of a blackout. The structural vulnerability of a power grids is addressed in [14] in the aftermath of the North American blackout in 2003. The structural vulnerability is investigated by means of a connectivity measurement, i.e. how the connectivity and hence the robustness of the power grid can decrease in a fast manner if significant buses are removed. It is concluded that cascading failures in particular have a devastating

impact on the connectivity. Expensive infrastructural investments are required to improve the structural deficiencies.

It was investigated in [15] how large interdependent networks like power grids can interact and failures in one network can lead to cascading failures in another network. Thus, the properties of interdependent network interaction should be considered when constructing robust systems. Geomagnetic disturbances originating from the solar activity [16] also pose a large threat to power grids or any other infrastructure including large conductors.

2.1 The Nature of the Blackout

The anatomy of a power grid blackout is explained in [11,17]. Generally, a scenario similar to the following is the usual lapse of events that finally results in a widespread blackout.

(i) **Stable state**
A power grid which is operated within its safe operating limits is considered. In many blackout cases the grid was weakened because of unusual high electric power demand, scheduled maintenance or large power import.

(ii) **Initial fault**
Somewhere in the grid one or several severe faults occurs such as short circuited lines or sudden loss of power generation. Such failures occur on a regular basis and should not adventure the general system operation.

(iii) **Counter measures**
The automatic protection system deals with the fault by utilizing appropriate counter-measures such as tripping of lines or generators and frequency or voltage stabilization by real and reactive power compensation. If the counter-measures are **insufficient**, the grid could be heading for **cascading failures**.

(iv) **Emergency state**
If cascading failures are avoided the grid is in a state of temporarily safe operation. The grid is built to survive at least one major failure due to the $N-1$-criterion [18] which implies that grid should withstand a worst case scenario of generator or line loss. Within minutes, the grid will return to a new operating point, i.e. to a new **Stable state**.

(v) **Unexpected fault**
If during the **Emergency state** another large, possibly uncorrelated failure occurs the grid could be heading for a state of **cascading failures**.

(vi) **Cascading stage**
During the cascading stage, tripping of lines or generators result in power flow overloads on neighboring transmission lines as well as voltage and frequency

fluctuations in the grid. Power flow overloads lead to further line disconnections due to protective relays and further disturbances are induced in the grid.

(vii) **Collapse**
At some point during the cascading stage, the grid will come to a *point of no return* where a partial or widespread blackout becomes inevitable. Due to voltage/frequency collapse or loss of synchronism between different areas, the grid will automatically be separated into isolated sub-grids. The sub-grid's ability to maintain the operation within acceptable limits determines if a blackout occurs or not. An important factor is the load-generation imbalance. If there is a large discrepancy in electric power demand and generation capability a blackout is likely to occur.

(viii) **Restoration**
In the aftermath of the blackout, the grid is scattered and heavily weakened. In the restoration process, generation are reconnected, frequency and voltage levels are stabilized and previously disconnected loads are gradually reconnected. Lastly, desynchronized areas are resynchronized.

Referring to the typical scenario outlined above, the 2003 blackout in Sweden will be shortly described [2, 11, 17]. The grid was considered to be operated under normal operating conditions. However, the grid was weakened due to maintenance of two 400 kV transmission lines as well as HVDC (high-voltage, direct current) lines connecting Sweden with the rest of Europe.

The first contingency, the **Initial fault** was the loss of a 1200 MW nuclear unit in Oskarshamn due to a steam valve problem. This event increased the power transfers from north to south. An **Unexpected fault** then occurred at a distance of only 300 km from the first outage. An equipment failure at a substation caused a double-bus fault which lead to the disconnection of two 900 MW nuclear plants. From here, a large deficiency in generation in the south part of Sweden caused overloaded lines and voltage instabilities, i.e. a **Cascading stage**. The only 400 kV line connecting south to north experienced a serious overload and consequently the the south part of Sweden and Denmark became islanded from the rest of the grid. With only a 30 % generation capability to cover the demand an instant blackout or **Collapse** unfolded.

2.2 Prevention Methods

The fundamental prerequisite in an AC power network is the synchronism of generators. Synchronism implies that all generators deliver power at a common system frequency f_s, 50 or 60 Hz. If one generator is not in synchronism with the system, power can not be delivered from the generator to the system. As a consequence to severe disturbances, generators can fall out of synchronism which is a major stability threat. Thus, a controlled islanding strategy should prevent generators from

falling out of synchronism. It was shown in [19] how optimal tuning of generator parameters enhance the synchronization and thus improves the robustness of the grid.

However, serious failures in the grid often also lead to load-generation imbalances causing the system frequency to decrease or increase, or inducing voltage fluctuations. Thus, many types of controls are used in a power grid to suppress these kind of disturbances and they operate at different time-scales.

In [11] it is described how large scale blackouts are currently prevented and future recommendations to avoid them are given. An IT infrastructure supporting wide-area measurements and control is mentioned as an important prevention measure. Controlled separation is suggested to deal with widespread failure and loss of synchronism between different areas in the grid. Maintenance, inspection and testing of existing hardware as well as replace old hardware are important safety measures to limit the occurrence of random equipment failures. Also, deeper understanding and research on cascading failures are required to construct even more efficient methods.

Wide-area measurements have been tested and researched on intensively in recent years. In [20], measurements from PMUs are incorporated in a Wide-Area stability and voltage Control System (WACS). The WACS is able to trip generators and provide measurements for control of power compensation. In [21] it is shown how WAMS can provide control input and increase the dynamic performance based on simulation of a real power grid.

Many strategies for *controlled islanding* have been suggested in the last decade. An illustrative image of a power grid separation is depicted in figure 2.1. The idea is to identify suitable boundaries where a separation is beneficial for the ability to withstand cascading failures and avoid a blackout. Often the usage of a WAMS is assumed and based on system measurements a decision of separation is being made.

A method based on the slow coherency of generators [22] has been suggested as an effective strategy of controlled islanding. Slow coherency is based on the two-time-scales method in dynamical system theory where the dynamics can be divided into fast and slow states. That is, slowly and rapidly changing dynamics. Groups of generators showing *coherency* are identified for the slow states and separation between the groups are identified with respect to a minimum load-generation imbalance within the considered islands. A coherent groups of generator shows coupled dynamics and the boundaries between these groups are hence considered as proper boundaries to split the grid. The lines connecting different groups are called *tie-lines* and through these *tie-lines* fast dynamics are propagated if the grid is not properly separated. It is reported in [23] that for the (in)famous 2003 blackout event in the United States, the slow coherency-based controlled islanding can improve the grid's performance substantially. Also, based on slow coherency or any preferred grouping method for generators, a minimal cut-set with a minimum net flow method was demonstrated in [24]. That is, to minimize the load-generation imbalance within the islands caused by the separation and thus avoid further disturbances induced by power flow redirections in the grid.

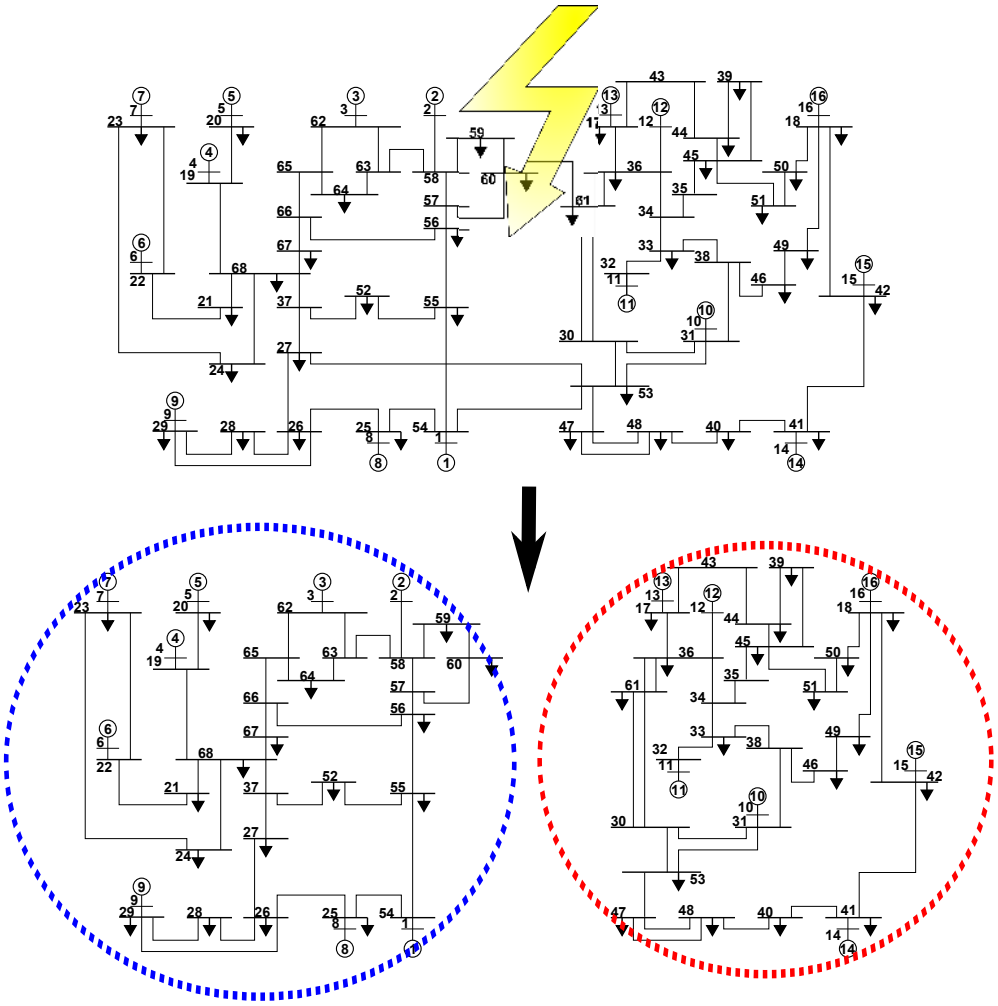

Figure 2.1: A controlled islanding strategy for a power grid determines appropriate separation boundaries and splits accordingly in case of severe or cascading failures with the purpose of avoiding a widespread blackout.

An islanding scheme using synchrophasors (e.g. PMUs) was proposed in [25]. It suggests measurements of generators and monitoring of the possible separation between different coherent groups of generators. Ordered Binary Decision Diagrams (OBDDs) are used to find the cut-set of transmission lines separating the grid into isolated parts. OBDD is a data structure representation of a network. An OBDD based controlled islanding strategy is utilized in [26] and evaluated by simulations in [27].

A popular method to study the properties of networks is by means of spectral

graph theory. In spectral graph theory, network properties are analyzed by the eigenvalues and eigenvectors of its matrix representation. It is obvious that the structure of the network, such as a power distributing network also affects the dynamic performance. In [28] a strategy is presented where a power grid is separated into different parts using the spectral graph theory. In this thesis, spectral graph theory will be compared to results from the KMA-based method which is a method based on measurements of dynamics of a power grid. The basic features of spectral graph theory is given in section 3.2.

Most of the existing strategies are based on linear systems theory and methodology. This thesis instead investigates the possibilities of an alternative method for power grid islanding which can fully capture nonlinear characteristics based only on a series of measurements. The theory used in the method is described in section 3.1 and the method is outlined in chapter 4.

Chapter 3

Mathematical Tools

3.1 Koopman Mode Analysis

Recently, the nonlinear Koopman Mode (KM) has been applied to power grid analysis [7, 8]. The so-called Koopman Mode Analysis (KMA) is a new technique of nonlinear modal decomposition based on properties of the point spectrum of the Koopman operator [5, 6]. By definition, each KM oscillates with a single frequency and is hence relevant for capturing the spatiotemporal pattern of the dynamics of a large-scale power grid. In [7] the relevant feature is exploited for coherency identification based on data of swing dynamics in every generator, meaning that in a coherent group of generators, all of them swing in phase with a common frequency.

The following theory is based on [6]. Consider the dynamics described by a discrete-time, nonlinear difference equation on a smooth manifold M:

$$\boldsymbol{x}_{k+1} = \boldsymbol{f}(\boldsymbol{x}_k), \tag{3.1}$$

where $\boldsymbol{f}$ is a nonlinear map from M to itself. The Koopman operator is a linear, infinite dimensional operator acting on a scalar function (*observable*) $g : M \to \mathbb{R}$ in the following manner:

$$Ug(\boldsymbol{x}) = g(\boldsymbol{f}(\boldsymbol{x})). \tag{3.2}$$

The eigenvalues $\lambda_j \in \mathbb{C}$ and eigenfunctions φ_j: $M \to \mathbb{C}$ are defined as

$$U\varphi_j(\boldsymbol{x}) = \lambda_j \varphi_j(\boldsymbol{x}), \qquad \text{for } j = 1, 2, \ldots \tag{3.3}$$

where λ_j is called the j-th Koopman eigenvalue. Here, let $\boldsymbol{g}$: $M \to \mathbb{R}^p$ be a vector-valued observable. If each g_i of the components in $\boldsymbol{g}$ lies within the span of eigenfunctions φ_j, then the time-evolution of observable $\boldsymbol{g}(\boldsymbol{x}_k)$ from $\boldsymbol{g}(\boldsymbol{x}_0)$ is expanded as follows:

$$\boldsymbol{g}(\boldsymbol{x}_k) = \sum_{j=1}^{\infty} U^k \varphi_j(\boldsymbol{x}_0)\boldsymbol{v}_j = \sum_{j=1}^{\infty} \lambda_j^k \varphi_j(\boldsymbol{x}_0)\boldsymbol{v}_j, \tag{3.4}$$

where $\boldsymbol{v}_j$ is the vector-valued coefficient of the decomposition and is called the j-th Koopman Mode (KM). This decomposition is based on properties of the point spectrum of U, and the analysis based on (3.4) is called the Koopman Mode Analysis (KMA).

3.1.1 Computation of Koopman Modes

Computation of Koopman eigenvalues and KMs is a challenging problem. A modified version of the Arnoldi algorithm described in [6] shows that the *Ritz* values $\tilde{\lambda}_j$ and vectors $\tilde{\boldsymbol{v}}_j$ approximate the Koopman eigenvalues λ_j and factors $\varphi_j(\boldsymbol{x}_0)\boldsymbol{v}_j$ in the expansion (3.4) in terms of a finite truncation. In other words, it is possible to decompose the measured dynamics in terms of a finite number of eigenvalues and eigenvectors ($\tilde{\lambda}_j$ and $\tilde{\boldsymbol{v}}_j$). The Ritz values and vectors are computed as follows.

Let's consider a set of N+1 vectors of data, $\{\boldsymbol{g}(\boldsymbol{x}_0), \ldots, \boldsymbol{g}(\boldsymbol{x}_N)\}$. $\boldsymbol{g}(\boldsymbol{x}_k)$ is a vector measuring some observables (e.g. generator frequency ω_i, $i = 1, \ldots, n$) at a certain time t_k. Then a residual $\boldsymbol{r}$ is defined as:

$$\boldsymbol{r} = \boldsymbol{g}(\boldsymbol{x}_N) - \sum_{j=0}^{N-1} c_j \boldsymbol{g}(\boldsymbol{x}_j), \tag{3.5}$$

and the constants c_j chosen such that

$$\boldsymbol{r} \perp \text{span}\{\boldsymbol{g}(\boldsymbol{x}_0), \ldots, \boldsymbol{g}(\boldsymbol{x}_{N-1})\}. \tag{3.6}$$

With $M = [\boldsymbol{g}(\boldsymbol{x}_0), \ldots, \boldsymbol{g}(\boldsymbol{x}_{N-1})]$ and $\boldsymbol{c} = [c_0, \ldots, c_{N-1}]$, (3.5) together with (3.6) gives

$$M^{\mathrm{T}}\boldsymbol{r} = \boldsymbol{0} = M^{\mathrm{T}}\boldsymbol{g}(\boldsymbol{x}_N) - M^{\mathrm{T}}M\boldsymbol{c}^{\mathrm{T}} = B - A\boldsymbol{c}, \tag{3.7}$$

and the constants $\boldsymbol{c}$ are consequently given by

$$\boldsymbol{c} = A^{\dagger}B, \tag{3.8}$$

where $A^{\dagger}$ is the Moore-Penrose pseudoinverse of A. The pseudoinverse or generalized inverse is defined for any $m \times n$ matrix and for the case of a non-square matrix ($m \neq n$) it includes a *best fit*, i.e. a least square approximation. With the obtained $\boldsymbol{c}$, let us now consider the companion matrix C:

$$\mathrm{C} = \begin{bmatrix} 0 & 0 & \ldots & 0 & c_0 \\ 1 & 0 & & 0 & c_1 \\ 0 & 1 & & 0 & c_2 \\ \vdots & & \ddots & & \vdots \\ 0 & 0 & \ldots & 1 & c_{N-1} \end{bmatrix} \tag{3.9}$$

The Ritz values $\tilde{\lambda}_j$ is now given by $\det(\mathrm{C} - \lambda \mathbb{1}) = 0$. The Vandermonde matrix is then defined as:

$$\mathrm{T} = \begin{bmatrix} 1 & \tilde{\lambda}_1 & \tilde{\lambda}_1^2 & \dots & \tilde{\lambda}_1^{N-1} \\ 1 & \tilde{\lambda}_2 & \tilde{\lambda}_2^2 & \dots & \tilde{\lambda}_2^{N-1} \\ \vdots & \vdots & \vdots & \ddots & \vdots \\ 1 & \tilde{\lambda}_1 & \tilde{\lambda}_N^2 & \dots & \tilde{\lambda}_N^{N-1} \end{bmatrix} \tag{3.10}$$

The Ritz vectors $\tilde{\boldsymbol{v}}_j$, i.e., an approximation of the Koopman modes, are defined as the columns of

$$\mathrm{V} = [\boldsymbol{g}(\boldsymbol{x}_0), \dots, \boldsymbol{g}(\boldsymbol{x}_{N-1})]\mathrm{T}^{-1}. \tag{3.11}$$

$\tilde{\lambda}_j$ and $\tilde{\boldsymbol{v}}_j$ behave like Koopman eigenvalues λ_j and term $\varphi_j(\boldsymbol{x}_0)\boldsymbol{v}_j$ for a finite sum compared to equation (3.4) shown before. In the following, $\tilde{\boldsymbol{v}}_j$ is called the Koopman Mode (KM). The input of the algorithm is the $N+1$ sampled data $\{\boldsymbol{g}(\boldsymbol{x}_0), \boldsymbol{g}(\boldsymbol{x}_1), \dots, \boldsymbol{g}(\boldsymbol{x}_N)\}$. The outputs are N Koopman eigenvalues and KMs. The finite sum expansion is expressed in (3.12) and (3.13):

$$\boldsymbol{g}(\boldsymbol{x}_k) = \sum_{j=1}^{N} \tilde{\lambda}_j^k \tilde{\boldsymbol{v}}_j, \quad k = 0, \dots, N-1, \tag{3.12}$$

$$\boldsymbol{g}(\boldsymbol{x}_N) = \sum_{j=1}^{N} \tilde{\lambda}_j^N \tilde{\boldsymbol{v}}_j + \boldsymbol{r}, \tag{3.13}$$

where $\boldsymbol{r}$ is a residue with the approximation error. By means of $\tilde{\lambda}_j$ and $\tilde{\boldsymbol{v}}_j$, the captured nonlinear dynamics are analyzed with an usually small approximation error.

3.1.2 Coherency in Koopman Modes

Here let us introduce the notion of coherency in KMs [7, 29]. A coherent group of KMs is identified based on the *amplitude coefficient* $A_{ji} := |\tilde{v}_{ji}|$ and *initial phase* $\alpha_{ji} := \arg(\tilde{v}_{ji})$ for each mode j and observable i (e.g. generator rotor speed ω_i or bus voltage angle θ_i). Coherency for KMs is defined in [29] as follows. For a finite number N of modes $\{\tilde{\boldsymbol{v}}_1, \dots, \tilde{\boldsymbol{v}}_N\}$ and constants (ϵ_1, ϵ_2), two observables $\{g_k, g_v\}$ are called (ϵ_1, ϵ_2)-coherent with respect to mode j if

(i) $|A_{j,k} - A_{j,v}| < \epsilon_1$,

(ii) $|\alpha_{j,k} - \alpha_{j,v}| < \epsilon_2$,

which is illustrated in figure 3.1. An alternative method for identifying coherent groups of observables is to apply the k-means clustering method.

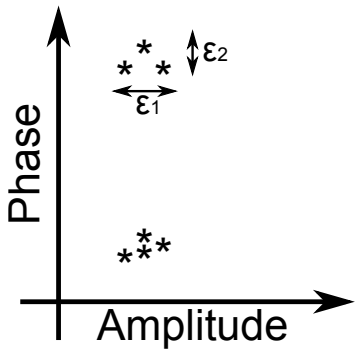

Figure 3.1: Groups of (ϵ_1, ϵ_2)-coherent observables illustrated in a phase vs. amplitude plot.

3.1.3 Simple KMA Example

Let us consider a simple illustrative example of KMA. The signals shown in (3.14) act as our measurements. Note that these signals have no coupling whatsoever.

$$g_1 = 0.5 \sin(2\pi f_1 t), \quad g_2 = 0.8 \sin(2\pi f_2 t - \pi/2), \quad g_3 = \sin(2\pi f_3 t). \tag{3.14}$$

Here $\{f_1, f_2, f_3\}$ are chosen as $\{6 \text{ Hz}, 2.6 \text{ Hz}, 0.7 \text{ Hz}\}$. The signals are depicted in figure 3.2 below for a time period of 4 s.

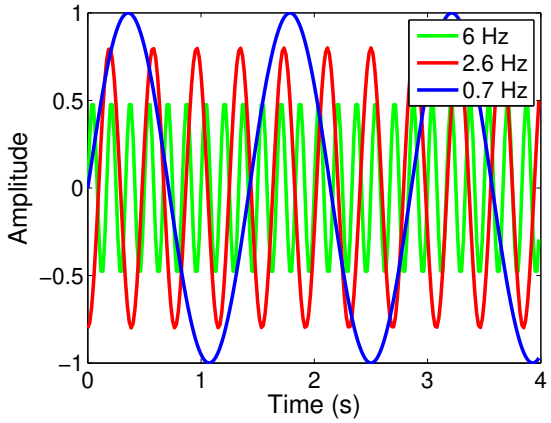

Figure 3.2: Three sine waves of different frequency corresponding to (3.14). The 2.6 Hz sine wave is displaced by a $\pi/2$ phase shift.

Let us now apply the KMA with a sampling frequency of $f_s = 60$ Hz to the data depicted in figure 3.2. $N + 1 = 240$ samples are acquired which gives $N = 239$ modes. The modes are now listed based on the Growth Rate (GR) $|\tilde{\lambda}_j|$ which is

related to the damping in case of sampled dynamics. In table 3.1 the ten modes with the largest GRs are listed.

Table 3.1: Dominant Koopman modes obtained for the data shown in figure 3.2. Colored frequencies are equal or close to the frequencies of the sine waves (g_1, g_2, g_3).

Mode j	GR $\lvert\tilde{\lambda}_j\rvert$	Freq. (Hz) $\mathrm{Im}[\ln\tilde{\lambda}_j]/(2\pi T_s)$	Norm $\lVert\tilde{\boldsymbol{v}}_j\rVert$
1	0.9997	0.68	0.0269
2	0.9960	2.66	0.2814
3	0.9951	5.94	0.0266
4	0.9925	0.39	0.5401
5	0.9913	0.13	0.1816
6	0.9898	0.99	0.3171
7	0.9897	2.93	0.0513
8	0.9894	2.34	0.1207
9	0.9893	6.25	0.2850
10	0.9892	5.67	0.1331

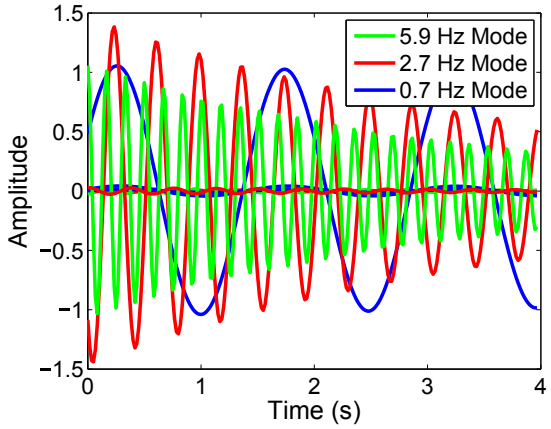

Figure 3.3: The modal "dynamics" of the three dominant modes. Each of the modes has three contributions corresponding to the three measured observables (the sine waves g_1, g_2, g_3).

In this manner, the sampled data has been decomposed into a set of Ritz values $\tilde{\lambda}_j$ and vectors $\tilde{\boldsymbol{v}}_j$. The dominant frequencies were identified by applying KMA to the sampled data. Modal dynamics for Mode 1-3 are depicted in figure 3.3. We see that for each mode, essentially only one observable (out of three) contributes (the one corresponding to the sine wave of the same frequency as the mode). The sum over all modes according to (3.12)-(3.13) reconstructs the sampled data.

3.2 Spectral Graph Theory

It is described in [28] how a power grid is split into islands based on spectral graph theory. For a given power grid with n buses connected via transmission lines, the grid is modeled as a graph with n vertices. The transmission lines connecting the buses are represented as edges of the graph. The graph is denoted as $\mathcal{G} = (V, E)$, where V is the set of vertices and E the set of edges connecting the vertices. An edge is denoted as a pair (u, v) of vertices. For $\mathcal{G}$, the adjacency matrix A [28] is introduced as

$$\mathsf{A}(u,v) = \begin{cases} 1, & \text{if } (u,v) \in E. \\ 0, & \text{otherwise.} \end{cases} \tag{3.15}$$

The degree d_i of a vertex is the sum of the i-th row of the adjacency matrix A, i.e. the number of edges connected to the vertex. The degree matrix D [28] is defined as a diagonal matrix given by

$$\mathsf{D} = \begin{cases} d_i, & \text{if } i = j. \\ 0, & \text{otherwise.} \end{cases} \tag{3.16}$$

Then, the Laplacian L [28] for $\mathcal{G}$ is defined as

$$\mathsf{L} = \mathsf{D} - \mathsf{A}. \tag{3.17}$$

The Laplacian L of $\mathcal{G}$ has the following properties for an unweighted or positively weighted graph [28]:

(i) L is symmetric and singular;

(ii) L has non-negative eigenvalues;

(iii) L is positive semi-definite.

The eigenvalues of L are conventionally listed by increasing magnitude, where the first eigenvalue λ_1 equals to zero. Thus, the eigenvalues are ordered in the following manner:

$$\lambda_1 = 0 \leq \lambda_2 \leq \ldots \leq \lambda_n.$$

It is shown in [30] that the second eigenvalue λ_2 and the corresponding eigenvector $\mathbf{V}_2$ contain important information about the connectivity of the graph. If $\lambda_2 = 0$, the graph is disconnected. The eigenvector $\mathbf{V}_2$ reveals information about the graph structure through the value of the components in $\mathbf{V}_2$. In [31] the partitioning properties of $\mathbf{V}_2$ are derived. For a fixed constant $k \leq 0$, it is shown that a collection of vertices C is connected if $[V_2]_i \geq k$ for all $i \in C$ where $[V_2]_i$ denotes the i-th element of $\mathbf{V}_2$. In [28] this property is used to determine a partition of power grid

for security enhancement in the following manner: Two groups of buses, $\boldsymbol{A}$ and $\boldsymbol{B}$ where $\boldsymbol{A} \cap \boldsymbol{B} = \varnothing$ and $\boldsymbol{A} \cup \boldsymbol{B} = \mathbf{V}_2$, are constructed as follows:

$$\begin{aligned} i \in \boldsymbol{A} \qquad & \text{if } [V_2]_i \geq 0, \\ i \in \boldsymbol{B} \qquad & \text{if } [V_2]_i < 0. \end{aligned} \tag{3.18}$$

As a simple, illustrative example let us consider the graph shown in figure 3.4.

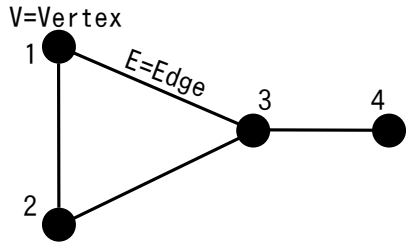

Figure 3.4: An example graph with four vertices and four edges connecting the vertices.

The graph Laplacian L is now calculated according to (3.17):

$$\mathsf{D}\left(=\begin{bmatrix} 2 & 0 & 0 & 0 \\ 0 & 2 & 0 & 0 \\ 0 & 0 & 3 & 0 \\ 0 & 0 & 0 & 1 \end{bmatrix}\right) - \mathsf{A}\left(=\begin{bmatrix} 0 & 1 & 1 & 0 \\ 1 & 0 & 1 & 0 \\ 1 & 1 & 0 & 1 \\ 0 & 0 & 1 & 0 \end{bmatrix}\right) = \mathsf{L}\left(=\begin{bmatrix} 2 & -1 & -1 & 0 \\ -1 & 2 & -1 & 0 \\ -1 & -1 & 3 & -1 \\ 0 & 0 & -1 & 1 \end{bmatrix}\right)$$

and the eigenvalues are given by

$$\det\left(\mathsf{L} - \lambda \mathbb{1}\right) = 0$$

and listed by increasing magnitude

$$\lambda_1 = 0 \leq \lambda_2 = 1 \leq \lambda_3 = 3 \leq \lambda_4 = 4.$$

The values $[V_2]_i$ for each vertex, $i = 1, \ldots, 4$ are shown in figure 3.5. Based on the result shown in figure 3.5 the graph is partitioned according to (3.18) and the partitioned graph is shown in figure 3.6. An appropriate partition according to spectral graph theory is to group the vertices as $\{1, 2, 3\}$ and $\{4\}$ which also involves the cut of a minimum amount of edges (one).

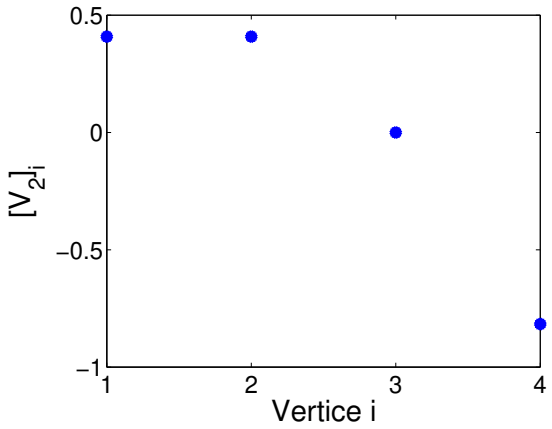

Figure 3.5: Values in second eigenvector $[V_2]_i$ is plotted for each vertex, $i = 1, \ldots, 4$ against the vertex number i.

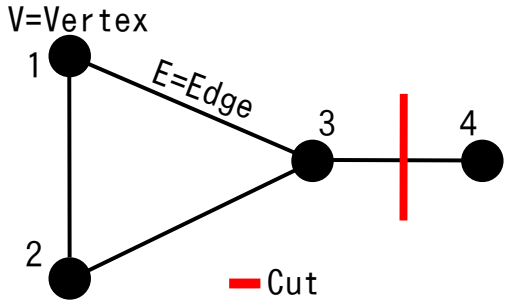

Figure 3.6: The example graph shown in figure 3.4 is partitioned according to (3.18).

Chapter 4

Koopman Mode Based Controlled Islanding Method

In this thesis the KMA is used for identification of coherent buses based on data on voltage angle dynamics of every bus that are obtained numerically by simulation or in practice with measurement units such as PMU [13]. Considering the coherency of buses (namely, node dynamics of a graph), cut-sets are determined for every partition. Splitting the power grid with respect to coherent groups is expected to form groups of buses with generators that are able to keep synchronism.

For a graph $\mathcal{G}$ constituting of disjoint v parts, a cut-set is the set of branches that upon removal separates $\mathcal{G}$ into $v + 1$ parts, and if all but one branch are removed, there is no separation [32]. Generally, the KMA captures well a local mode for dynamics of a single generator, an inter-machine mode for multiple generators or an inter-area oscillation [7]. Modes excited in the grid highly depend on the type of disturbance. In particular, when the grid responds to a severe disturbance, the dynamics of the grid show highly nonlinear features and can not be evaluated with the standard modal decomposition. Since cascading failures are typical of nonlinear multi-scale dynamics of a large-scale power grid, it is inevitable to consider multiple nonlinear modes that precisely capture the multi-scale dynamics.

4.1 Method

The outline of the method is as follows:

1. For measured data on voltage angle dynamics of every bus, the KMA is performed (see section 3.1 for details).

2. Coherent groups of buses are identified in terms of multiple KMs, which are dominant frequencies in the dynamics.

3. A partition of the power grid is derived based on the coherent groups of buses.

4. A cut-set for each partition is identified as a set of lines connecting different islanded sub-grids.

The proposed method has two novel points in comparison with the previously mentioned [22–24, 26–28, 33]. First, as mentioned above, the method is solely based on measurements of dynamics. In the controlled islanding, the target grid is highly transient and far from a steady state operating condition. Thus, it is questionable whether the grid partitioning based on static properties of the grid is effective. Interestingly, in Section 5.4, it is shown that the connectivity measure obtained from spectral graph theory, which comes from the static properties, is obtained with the dynamics-based method. Second, the proposed method is based on nonlinear dynamics of grids. The KMA is is capable of capturing nonlinear responses following a severe disturbance [7, 8], i.e. a mixture of local modes for dynamics of single generators, inter-machine modes for multiple generators or inter-area oscillations. Thus, it is expected that the proposed method based on the KMA provides an effective partition of a grid.

Chapter 5

Simulations and Results

5.1 Test Systems and Simulation Setting

5.1.1 Test Systems

Two IEEE test systems are used to evaluate the performance of the proposed strategy. Data for both test systems are available in [34].

The IEEE 68-bus test system contains 68 buses and 16 generators and is an interconnected network consisting of models of the New England Test System (NETS) and the New York Power System (NYPS) as shown in figure 5.1(a): see [35] for details.

The IEEE 118-bus test system represents a part of the American Electric Power System in 1962. It has been used in numerous studies as a test case, e.g. [1, 36–38]. The system dynamics are simulated with classical model for the 19 generators with parameters chosen same as in [27].

5.1.2 Simulation Setting

The dynamics of the test systems are simulated using the free open-source toolbox PSAT [10] for MATLAB. The mathematical model of the systems of differential and algebraic equations solved in PSAT are given in appendix A.1.

The KMA will be performed on data of generator dynamics ω and bus voltage angle dynamics θ for both test systems. $N + 1$ samples are collected with the sampling frequency $f_s = 60$ Hz. In a real power grid where measurements are obtained from PMU:s, 60 Hz is an appropriate sampling frequency [39].

For $N+1$ samples, N KMs are obtained. The dominant modes are identified by sorting them on the Growth Rate (GR) $|\tilde{\lambda}_j|$. The GR represents the damping of the mode and the norm $\|\tilde{\boldsymbol{v}}_j\|$ gives the magnitude of the contribution in the dynamics. A GR smaller than unity implies a positively damped mode. Based on the bus coherency of dominant modes, partitions for the grid are identified.

For both test-systems, splitting of the power system is conducted based on the partitions derived and the impact on the grid's response is investigated. The main

purpose of a controlled islanding is to relieve the stress of the grid and avoid an instability phenomenon (such as loss of synchronism of generators). To evaluate the control performance, it is inevitable to execute time-domain simulations of the grid with and without controlled islanding. It is assumed that the grid is operated at a steady operating condition before a disturbance. Then, the dynamics of the grid following the disturbance at a fault time t_{f} are simulated. The disturbance is cleared at a pre-defined time t_{c}, called the clearing time. As t_{c} increases, the grid's response (e.g. generator angles and frequencies) tends to increase and finally begins to diverge. The critical t_{c}, where the response begins to diverge, is called the critical clearing time t_{cc} [18].

An important parameter in a controlled islanding strategy is the separation timing. In this investigation, the separation time t_{sep} is fixed at 20 cycles after the fault clearing t_{c}, i.e.:

$$t_{\mathrm{sep}} = t_{\mathrm{f}} + t_{\mathrm{c}} + 20/f_{\mathrm{s}}.$$

This lies within the range of normal relay and circuit breaker interrupting times [40].

5.1.3 Power System Stability

There are three main stability classifications for power systems. Most fundamental is the ability of generators to maintain in synchronism with each other. This is commonly referred to as *rotor angle stability*. A case of such instability usually occurs within seconds (0 - 10 s) after a fault [40]. The study of rotor angle stability by applying large faults is known as *transient stability*. **For the test cases studied in this thesis, transient stability investigated, i.e. the ability to maintain the synchronism between generators in the post-islanding setting**.

The second type of stability is voltage stability which is the ability of the system to maintain voltages within acceptable limits after and during the occurrence of faults. Voltage stability is closely linked to reactive power.

The third type is frequency stability. There are severe restrictions for the allowed system frequency in the system. The frequency should be kept almost constant not to damage or impair performance of generators and other equipment designed for the system frequency. Frequency stability is closely linked to real power.

See the popular book by P. Kundur [40], for definitions and extensive descriptions of power system stability and control.

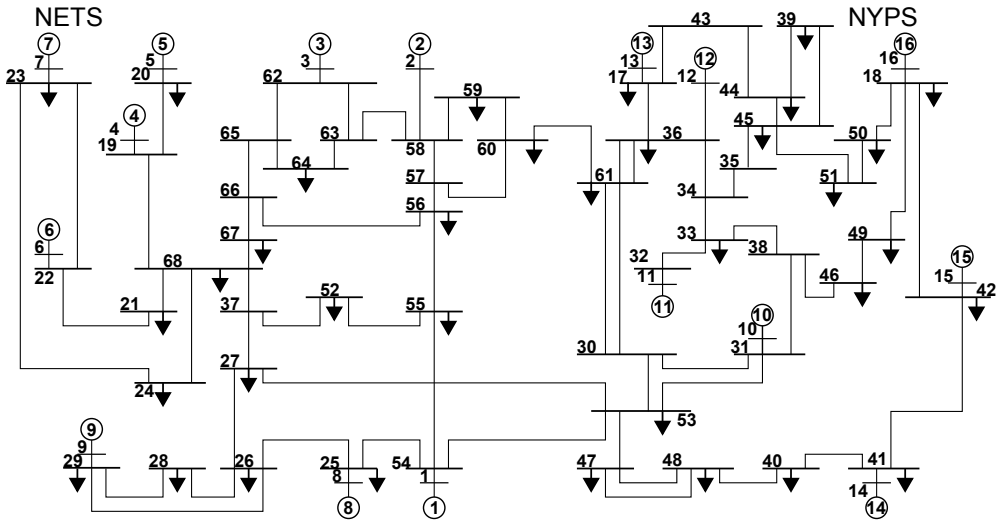

(a) IEEE 68-bus test system

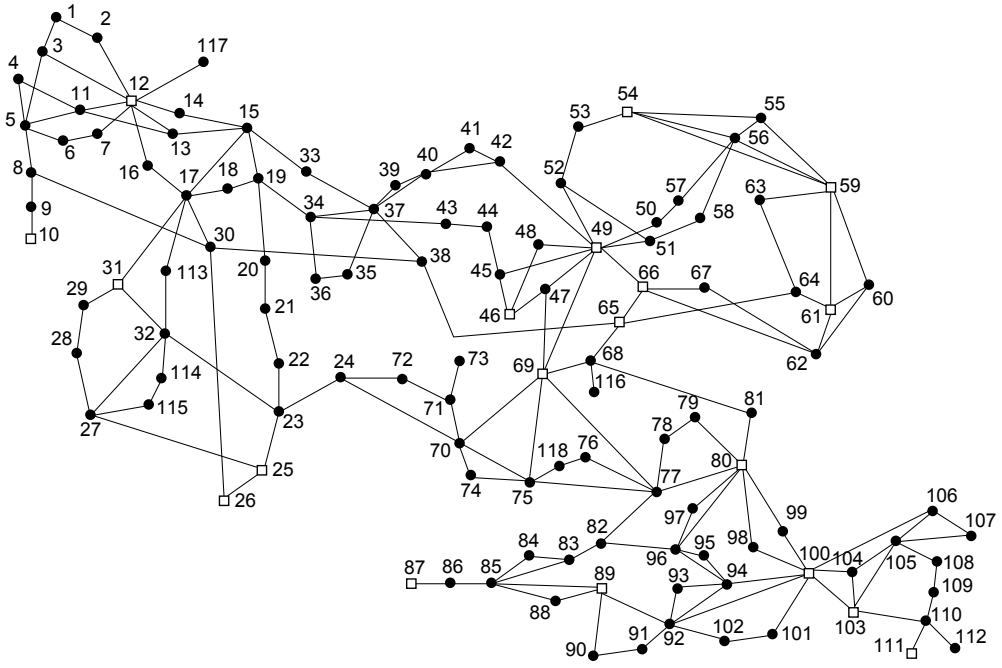

(b) IEEE 118-bus test system

Figure 5.1: (a) IEEE 68-bus test system. This system is an interconnection of two sub-systems called NETS (New England Test System) and NYPS (New York Power System) (b) IEEE 118-bus test system. The dynamics of the system is simulated with the classical model of 19 generators. Generator buses are indicated by hollow squares and filled circles represents load buses.

5.2 Test Case - IEEE 68-Bus Test System

The following disturbance is applied in this analysis:

Fault-case 68 A three-phase fault is applied close to bus 60 at $t_f = 1$ s with a clearing time $t_c = 124$ ms. The fault is cleared by disconnecting the line between bus 60 and 59. The line is then reconnected at $t = 1.5$ s.

5.2.1 Linear Modes and Koopman Modes

Let us first compare KMs to Linear Modes (LMs) by analyzing the dynamics of generators. The ten least damped pairs of LMs are given in table 5.1. LMs are calculated with PSAT: see Appendix A.3 for mathematical details. The oscillatory LMs are complex conjugate pairs $\lambda_j = \sigma_j \pm j\omega_j$ obtained from the linearization of the system of differential equations describing the dynamics.

KMA is applied to the dynamics of generator angular frequencies ω_i, $i = 1, \ldots, 16$, in the post-fault dynamics induced by the three-phase fault disturbance (***Fault-case 68***). $N + 1 = 481$ samples are collected during 8 s in the post fault dynamics and 480 KMs are obtained. The dynamics are shown in figure 5.2 and ten KMs are given in table 5.1 and listed by decreasing GR. In figure 5.3, the Koopman eigenvalues $\tilde{\lambda}$ are plotted in the complex plane.

A comparison between the frequencies appearing among LMs and KMs tells that multiple frequencies are identical or similar. Similar or equal frequencies for the two types of modes are highlighted by the same color.

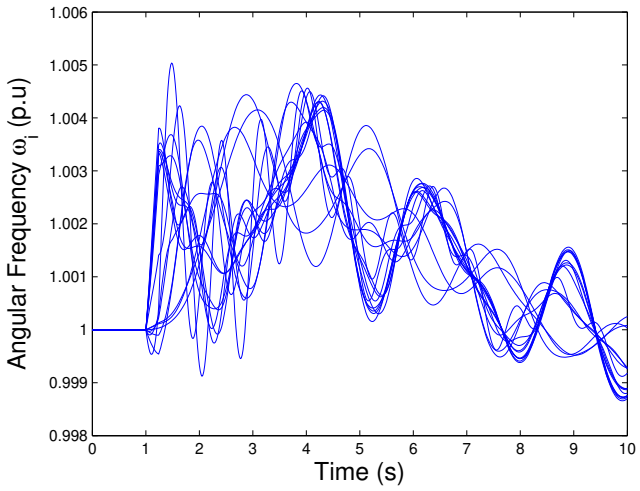

Figure 5.2: Generator angular angular frequency dynamics in the IEEE 68-bus test system following the three-phase fault on bus 60.

Table 5.1: Poorly damped linear modes obtained from small signal analysis are listed to the left. Koopman modes obtained for data on generator frequency dynamics in figure 5.2 are listed to the right. Equally colored frequencies are those frequencies found among both types of modes (with exception of white that indicates unique frequencies).

Linear Modes			Koopman Modes			
Mode j	Damping $-\sigma_j/\lvert\lambda_j\rvert$	Freq. (Hz) $\omega_j/(2\pi)$	Mode j	GR $\lvert\tilde{\lambda}_j\rvert$	Freq. (Hz) $\mathrm{Im}[\ln\tilde{\lambda}_j]/(2\pi T_s)$	Norm $\lVert\tilde{\boldsymbol{v}}_j\rVert$
1	0.0394	±1.33	1	1.0000	0	16.1
2	0.0394	±1.26	2	0.9982	0.84	$1.8 \cdot 10^{-7}$
3	0.0441	±0.54	3	0.9960	0.56	$2.6 \cdot 10^{-6}$
4	0.0460	±1.83	4	0.9952	0.98	$4.50 \cdot 10^{-7}$
5	0.0466	±0.64	5	0.9952	1.56	$2.06 \cdot 10^{-7}$
6	0.0468	±1.13	6	0.9950	0.69	$1.14 \cdot 10^{-5}$
7	0.0477	±1.07	7	0.9950	0.17	$7.19 \cdot 10^{-6}$
8	0.0481	±0.41	8	0.9949	1.29	$2.91 \cdot 10^{-6}$
9	0.0488	±0.98	9	0.9946	1.73	$4.44 \cdot 10^{-8}$
10	0.0491	±1.53	10	0.9945	0.43	$8.11 \cdot 10^{-5}$

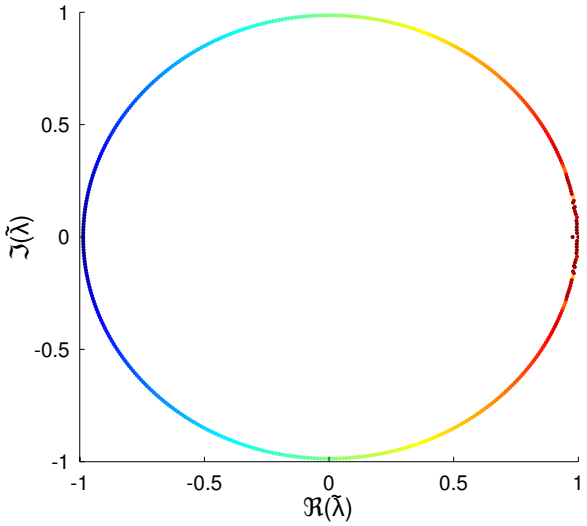

Figure 5.3: Koopman eigenvalues plotted with the imaginary part ($\Im(\tilde{\lambda}_j)$) against the real part ($\Re(\tilde{\lambda}_j)$). The modes are distributed close to the unit circle and are colored from red (largest norms) to blue (smallest norms).

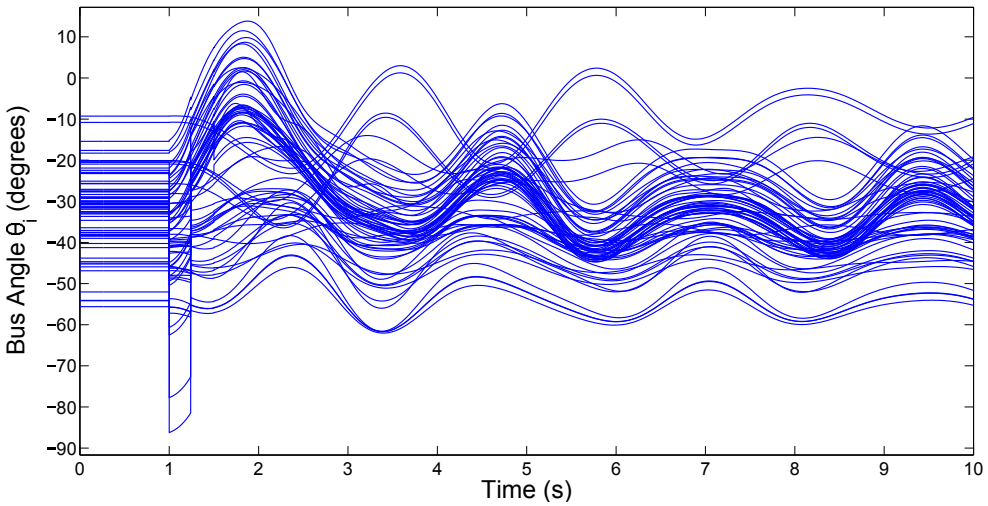

Figure 5.4: Voltage angle dynamics of buses in the IEEE 68-bus test system following the three-phase fault on bus 60. The bus angle dynamics are here shown in the Center Of Intertia (COI) reference frame (see appendix A.2).

5.2.2 Coherency Identification and Grid Partitioning

For the same fault case (***Fault-case 68***), the KMA is now performed for data on voltage angle dynamics of the 68 buses, θ_l, $l = 1, \ldots, 68$ shown in figure 5.4. The number of samples is $N + 1 = 481$ and N KMs are obtained. Ten KMs are listed in table 5.2 and are sorted based on decreasing GR. A comparison to the modal frequencies identified in table 5.1 reveals that two frequencies (≈0.67 Hz, ≈0.41 Hz) appear among both LMs as well as KMs for generator dynamics, (≈0.83 Hz, ≈1.78 Hz) only among the KMs and (≈1.13 Hz) only among the LMs. In other words, fundamental modal frequencies such as inter-area oscillations (oscillations between different parts of the system) and local mode dynamics are identified by analyzing the bus dynamics.

Now, based on the KMA of voltage angle dynamics, coherent groups of buses are identified and partitions are determined for the IEEE 68-bus test system.

Considering the modes listed in table 5.2. Mode 1 (0 Hz) and Mode 2 (0 Hz) represents the Non-Oscillatory (NO) or time-averaged dynamics of the grid. Mode 1 has a GR larger than unity whereas the GR of Mode 4 is equal to unity. More precisely, Mode 2 represents the average output of the observables. Mode 1, or the second NO mode $\tilde{\boldsymbol{v}}_{\mathrm{NO2}}$ will be investigated for the ***Case 2*** disturbance for the IEEE 118-bus test system.

Because Mode 3 and Mode 6 have large GRs as well as norms, they are regarded as dominant modes that capture the oscillatory response well. The initial phase α_{ji} versus the amplitude A_{ji} is plotted for every bus $i = 1, \ldots, 68$ in figures 5.5(a) and

Table 5.2: Dominant Koopman modes obtained for the data on voltage angle dynamics in figure 5.4. Colored frequencies are equal or close to frequencies identified for generator dynamics displayed in table 5.1 and hence share the same color.

Mode j	GR $\lvert\tilde{\lambda}_j\rvert$	Freq. (Hz) $\mathrm{Im}[\ln\tilde{\lambda}_j]/(2\pi T_s)$	Norm $\lVert\tilde{\boldsymbol{v}}_j\rVert$
1	1.0095	0	$8.14 \cdot 10^{-4}$
2	1.0000	0	$1.93 \cdot 10^{3}$
3	0.9989	0.67	$2.18 \cdot 10^{-2}$
4	0.9983	1.78	$2.45 \cdot 10^{-6}$
5	0.9981	2.47	$2.93 \cdot 10^{-7}$
6	0.9976	0.41	1.33
7	0.9973	2.61	$4.20 \cdot 10^{-7}$
8	0.9972	0.83	$5.13 \cdot 10^{-5}$
9	0.9971	2.33	$8.73 \cdot 10^{-7}$
10	0.9968	1.13	$4.45 \cdot 10^{-4}$

5.5(b) for Mode 1 and Mode 2, respectively. Clusters of buses are identified in terms of phase coherency and correspond to coherent groups of buses with respect to KMs as discussed below.

Grouping of buses based on Mode 3 in figure 5.5(b) leads to three groups of buses. One group corresponds to the NETS. NYPS is divided into two sub-groups: one group is large and contains most of the NYPS; the other group is small and corresponds to the north-east part of NYPS. The associated partition of the grid is shown in figure 5.7.

Grouping of buses based on Mode 6 in figure 5.5(a) leads to one large group and one smaller group. The latter group consists of the far-east buses in the NYPS system, and the former group represents the rest of the system. The associated partition of the grid is shown in figure 5.7.

A *fine partition* is constructed by considering at least two partitions and let the cut-set be the combination of cut-sets as illustrated in figure 5.6. By combining the partitions for Mode 3 and Mode 6, a partition with four disjoint parts are obtained. Partitions based on the concept of fine partition are multiple coherent for at least 2 frequencies and hence expect to keep generators in synchronism within the islands.

The graph theoretical partition is calculated according to (3.18). The resulting partition is shown in figure 5.7 and corresponds to the interconnection between NETS and NYPS.

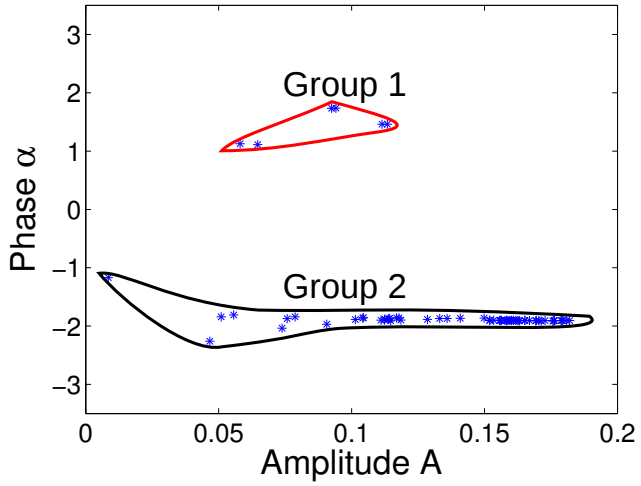

(a) Phase vs. amplitude plot (Mode 3)

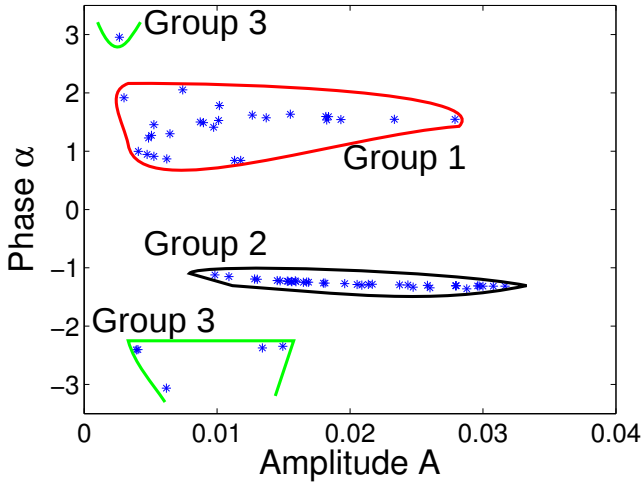

(b) Phase vs. amplitude plot (Mode 6)

Figure 5.5: (a) Phase vs. amplitude plot of buses for Mode 3 (0.67 Hz) and (b) Mode 6 (0.41 Hz).

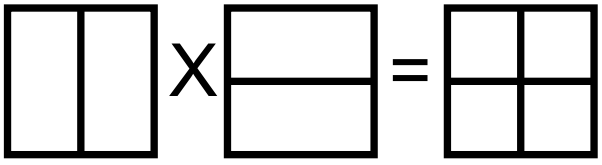

Figure 5.6: The concept of a fine partition. Here, a fine partition is constructed based on two partitions.

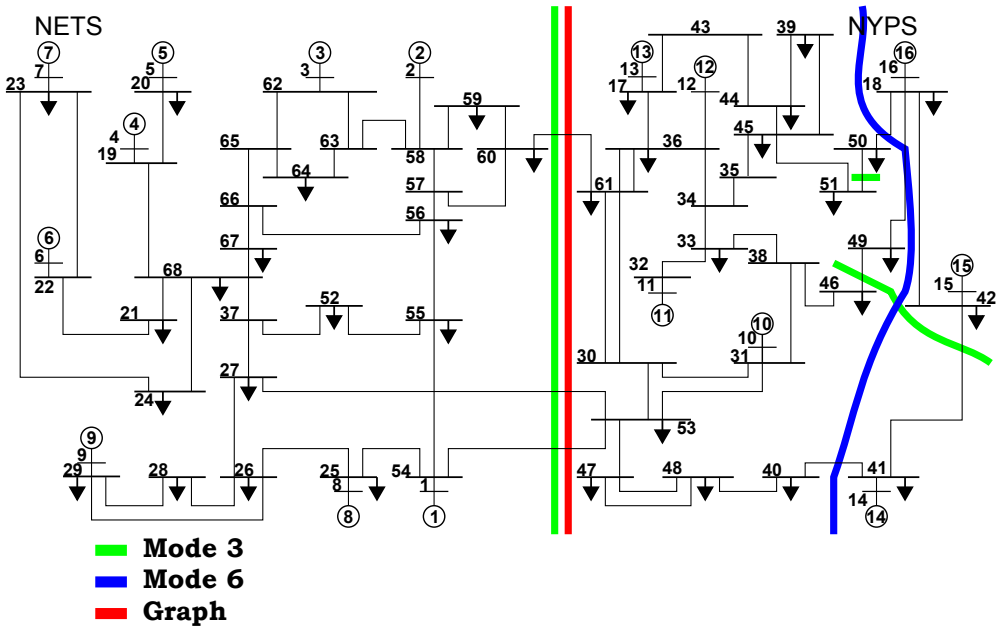

Figure 5.7: Partitioning of the IEEE 68-bus test system according to Mode 3, Mode 6 and spectral graph theory. The cut-sets are indicated by colored lines.

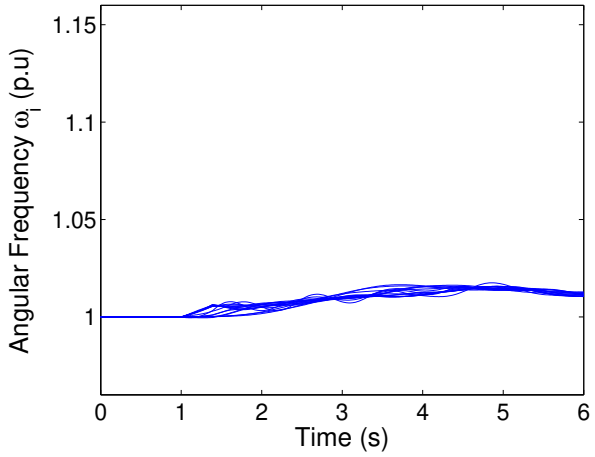

(a) $t_c = 390$ ms $< t_{cc}$

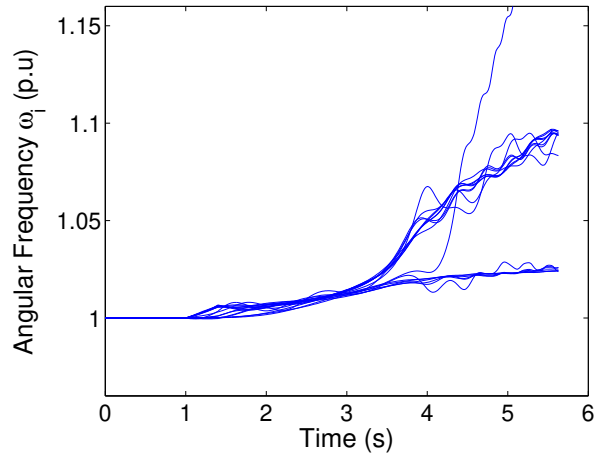

(b) $t_c = 400$ ms $> t_{cc}$

Figure 5.8: Angular frequency response for generators following a three-phase fault at bus 60 with (a) $t_c = 390$ ms and (b) $t_c = 400$ ms.

5.2.3 Time-Domain Simulations of Grid Splitting

For the ***Fault-case 68***, t_c is increased until a case of instability (divergence of generator frequencies) is achieved and t_{cc} is identified as ≈ 392 ms. The dynamics for angular frequencies of generators for $t_c = 390$ ms $< t_{cc}$ and $t_c = 400$ ms $> t_{cc}$ are depicted in figures 5.8(a) and 5.8(b), where a typical case of *step-out* of generators is observed in figure 5.8(b).

In the post-fault dynamics induced by the unstable disturbance ($t_c = 400$ ms)

the grid is now separated according to the partitions obtained from the two dominant modes (Mode 3 and 6), the fine partition and the graph theory partition. The data for the cut-sets are given in table 5.3.

The dynamic responses for the four cases are shown in figure 5.9. Instabilities similar to the unstable case shown in figure 5.8(b) are obtained for figure 5.9(a)-5.9(c) corresponding to the cut-sets obtained for KMA. However, the time-duration until the instability occurs varies. For the response of the Mode-3-splitting shown in figure 5.9(a), loss of synchronism is apparent short after the grid separation and finally the simulation is terminated at $t \approx 9$ s due to divergence. In figure 5.9(b) for the Mode 6 partition, the two groups of generators keep synchronism until $\approx$ 12 s until divergence of one generator occurs. Figure 5.9(c) shows the response of the separation for the fine partition (combination of Mode 3 and 6) and synchronism is here maintained until $\approx$ 15 s.

The response for the cut-set obtained from the graph theoretical partitioning shown in figure 5.9(d) stabilizes into two separate system frequencies (caused by the load-generation imbalance).

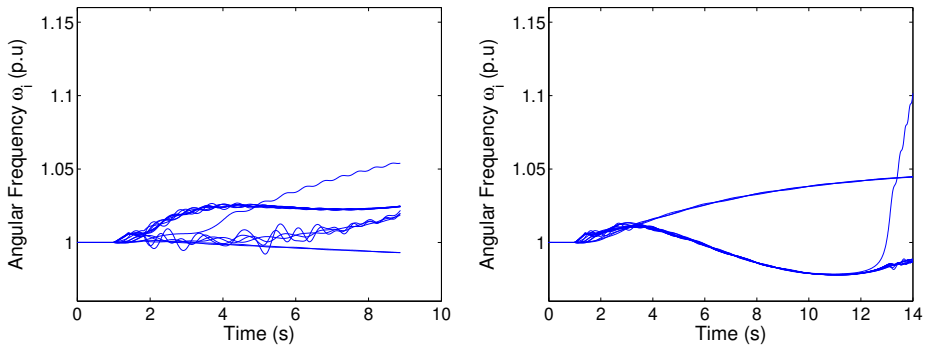

(a) Mode 3

(b) Mode 6

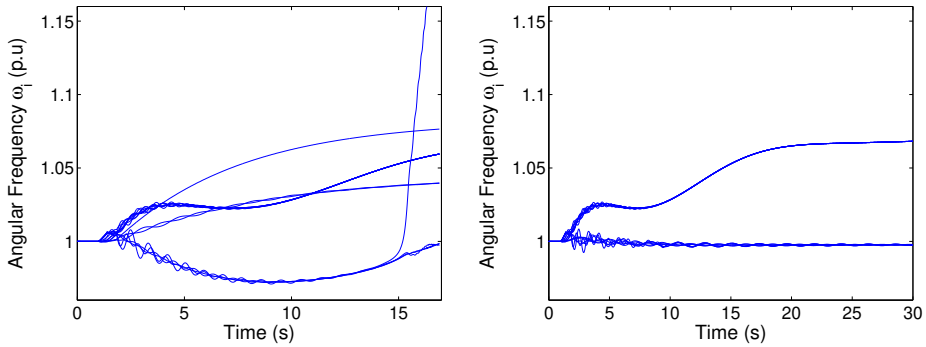

(c) Fine Partition

(d) Graph Theory - NETS-NYPS

Figure 5.9: Four different partitions are investigated during the event of a large fault and the test system is split according to (a) Mode 3, (b) Mode 6, (c) fine partition and (d) spectral graph theory.

Table 5.3: The data of the cut-sets illustrated in figure 5.7. The tie-lines are the lines connecting two groups of buses and a line is denoted in the table as $(b_{\text{fr}}, b_{\text{to}})$, where b_{fr} is the *from-bus* and b_{to} is the *to-bus*. $\Delta P_{\text{X}\to\text{Y}}$ is the power mismatch in Group X caused by disconnecting the tie-lines from Group X (Gr. X) to group Y where a positive sign (+) implies that power are being exported from Gr. X to Gr. Y. $\Delta P/G_{\text{tot}}$ is the power mismatch divided by the sum of the real power output of the generators in the group.

Cut-set	Tie-lines $(b_{\text{fr}}, b_{\text{to}})$	Generators	$\Delta P/G_{\text{tot}}$
Mode 3	(60,61), (53,27), (53,54), (45,51), (46,49), (42,41)	**Gr. 1:** {1,2,3,4,5, 6,7,8,9} **Gr. 2:** {10,11,12, 13,14} **Gr. 3:** {15,16}	**Gr. 1:** $\Delta P_{1\to2} = 7.13$ $\Delta P_{1\to2}/G_{\text{tot1}} = +13.8$ % **Gr. 2:** $\Delta P_{2\to1,3} = -11.77$ $\Delta P_{2\to1,3}/G_{\text{tot2}} = -14.3$ % **Gr. 3:** $\Delta P_{3\to2} = 4.64$ $\Delta P_{3\to2}/G_{\text{tot3}} = +10.6$ %
Mode 6	(50,18), (49,18), (41,40)	**Gr. 1:** {1,2,3,4,5, 6,7,8,9,10,11,12,13} **Gr. 2:** {14,15,16}	**Gr. 1:** $\Delta P_{1\to2} = -15.09$ $\Delta P_{1\to2}/G_{\text{tot1}} = -13$ % **Gr. 2:** $\Delta P_{2\to1} = 15.09$ $\Delta P_{2\to1}/G_{\text{tot2}} = +24.6$ %
Fine Part.	Mode 3 & 6's tie-lines	**Gr. 1:** {1,2,3,4,5, 6,7,8,9} **Gr. 2:** {10,11,12, 13} **Gr. 3:** {14} **Gr. 4:** {15,16}	**Gr. 1:** $\Delta P_{1\to2} = 7.13$ $\Delta P_{1\to2}/G_{\text{tot1}} = +13.8$ % **Gr. 2:** $\Delta P_{2\to1,3,4} = -19.58$ $\Delta P_{2\to1,3,4}/G_{\text{tot2}} = -30.4$ % **Gr. 3:** $\Delta P_{3\to2,4} = 7.81$ $\Delta P_{3\to2,4}/G_{\text{tot3}} = +43.8$ % **Gr. 4:** $\Delta P_{4\to2,3} = 13.08$ $\Delta P_{4\to2,3}/G_{\text{tot4}} = +30.1$ %
Graph Th.	(60,61), (53,27), (53,54)	**Gr. 1:** {1,2,3,4,5, 6,7,8,9} **Gr. 2:** {10,11,12, 13,14,15,16}	**Gr. 1:** $\Delta P_{1\to2} = 7.13$ $\Delta P_{1\to2}/G_{\text{tot1}} = +13.8$ % **Gr. 2:** $\Delta P_{2\to1} = -7.13$ $\Delta P_{2\to1}/G_{\text{tot2}} = -5.7$ %

5.3 Test Case - IEEE 118-Bus Test System

For this test system, two cases of disturbances are considered:

Case 1 A three-phase fault is applied to bus 68 with a clearing time $t_c = 350$ ms, slightly below critical clearing time $t_{cc} \approx 360$ ms.
Case 2 For initial generator frequency deviation ω_i^0, $i = 1, \ldots, 19$, the disturbance is initiated as $\omega_i^0 = \omega_i^0 + \Delta\omega_i$ where

$$\Delta\omega_i = \begin{cases} -0.001 \text{ p.u.}, & \text{if } i \text{ is odd}, \\ +0.001 \text{ p.u.}, & \text{if } i \text{ is even}. \end{cases} \tag{5.1}$$

5.3.1 Linear Modes and Koopman Modes

In the same manner as for the IEEE 68-bus test case, KMs are compared to Linear Modes (LMs) by analyzing the dynamics of generator frequencies ω_i for the ***Case 1*** fault. The dynamic response is shown in figure 5.10. $N + 1 = 481$ samples are collected during 8 s in the post faults dynamics which gives 480 KMs. The dominant KMs and poorly damped LMs are given in table 5.4. In figure 5.11, the Koopman eigenvalues $\tilde{\lambda}$ are plotted in the complex plane.

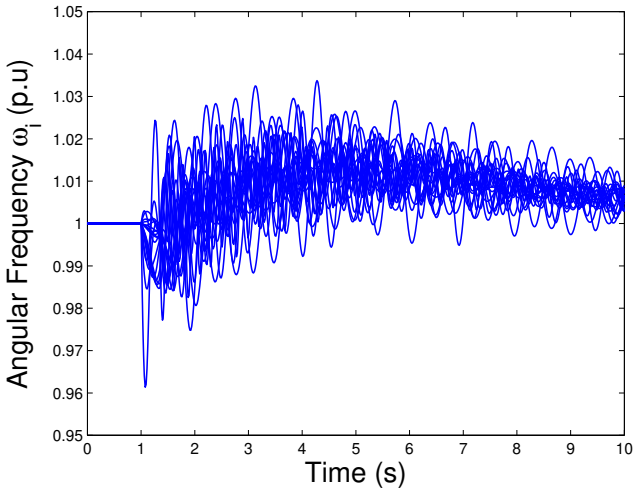

Figure 5.10: Angular angular frequency dynamics in the IEEE 118-bus test system for all 19 generators following the ***Case 1*** fault.

Table 5.4: Poorly damped linear modes obtained from small signal analysis are listed to the left. Koopman modes obtained for data on generator frequency dynamics in figure 5.10 are listed to the right. Equally colored frequencies are those frequencies found among both types of modes (with exception of white that indicates unique frequencies).

Linear Modes			Koopman Modes			
Mode j	Damping $-\sigma_j/\lvert\lambda_j\rvert$	Freq. (Hz) $\omega_j/(2\pi)$	Mode j	GR $\lvert\tilde{\lambda}_j\rvert$	Freq. (Hz) $\mathrm{Im}[\ln\tilde{\lambda}_j]/(2\pi T_s)$	Norm $\lVert\tilde{\boldsymbol{v}}_j\rVert$
1	0.0082	±4.17	1	1.0000	0	19.4536
2	0.0087	±5.20	2	0.9982	1.37	$2.02 \cdot 10^{-4}$
3	0.0093	±4.56	3	0.9980	1.20	$5.03 \cdot 10^{-5}$
4	0.0097	±3.41	4	0.9976	1.81	$2.43 \cdot 10^{-5}$
5	0.0107	±3.47	5	0.9973	1.55	$2.20 \cdot 10^{-4}$
6	0.0108	±2.78	6	0.9971	2.69	$3.59 \cdot 10^{-5}$
7	0.0115	±2.67	7	0.9969	1.97	$3.58 \cdot 10^{-5}$
8	0.0116	±3.84	8	0.9960	2.14	$9.41 \cdot 10^{-5}$
9	0.0120	±2.59	9	0.9958	1.05	$1.97 \cdot 10^{-4}$
10	0.0129	±2.06	10	0.9950	0.17	$1.09 \cdot 10^{-5}$

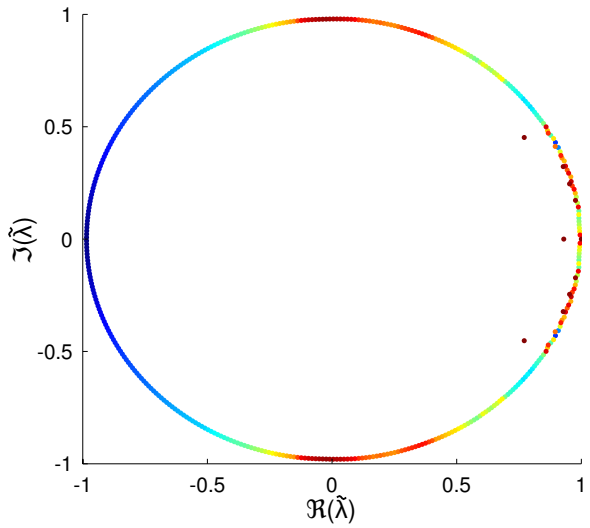

Figure 5.11: Koopman eigenvalues plotted with the imaginary part ($\Im(\tilde{\lambda}_j)$) against the real part ($\Re(\tilde{\lambda}_j)$). The modes are distributed close to the unit circle and are colored from red (largest norms) to blue (smallest norms).

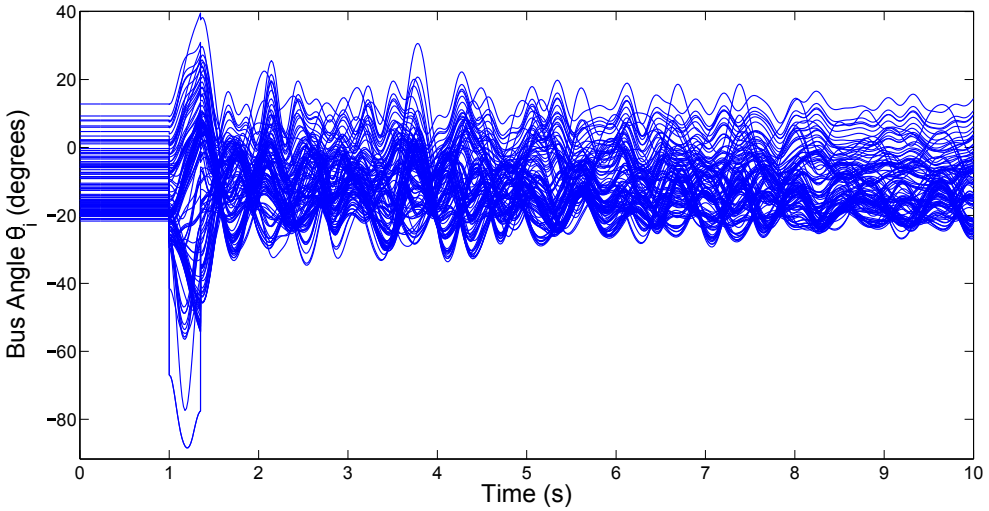

Figure 5.12: Voltage angle dynamics of buses in the IEEE 118-bus test system following a three-phase fault according to ***Case 1***. The bus angle dynamics are here shown in the Center Of Intertia (COI) reference frame (see appendix A.2).

5.3.2 Coherency Identification and Grid Partitioning

Now, based on the KMA of voltage angle dynamics for ***Case 1***, coherent groups of buses and associated partitions for the IEEE 118-bus test system are identified. $N = 420$ KMs are collected from the data displayed in figure 5.12 which corresponds to 7 s in the post fault dynamics, where the large excursions of bus angle swings are observed. Ten KMs are listed in table 5.5 and sorted based on decreasing GR.

Let us now consider the modes listed in table 5.5. Mode 1 (0 Hz) and Mode 4 (0 Hz) represents the Non-Oscillatory (NO) or time-averaged dynamics of the grid. Mode 1 has a GR equal to unity whereas the GR of Mode 4 is less than unity. Mode 1 represents the average output of the observables. Mode 4, or the second NO mode $\tilde{\boldsymbol{v}}_{\mathrm{NO2}}$ will be investigated for the ***Case 2*** disturbance.

Mode 2 (1.04 Hz) and Mode 3 (1.72 Hz) hold the largest GRs as well as norms among the oscillatory modes. Because Mode 2 and 3 have large GRs as well as norms, they are regarded as dominant modes that capture the oscillatory response well. The initial phase α_{ji} versus the amplitude A_{ji} is plotted for every bus $i = 1, \ldots, 118$ in Figs. 5.13(a) and 5.13(b) for Mode 2 and Mode 3, respectively. Several clusters of buses are identified in terms of phase coherency and correspond to coherent groups of buses with respect to KMs as described below. A k-means clustering algorithm can alternatively be used for clustering.

Grouping of buses based on Mode 2 in figure 5.13(a) leads to one large group and one smaller group. For Mode 3 (see figure 5.13(b)), two more equally sized groups are obtained as well as two isolated generator buses incoherent with the

Table 5.5: Dominant Koopman modes obtained for the data on voltage angle dynamics in figure 5.12. Colored frequencies are equal or close to frequencies identified for generator dynamics displayed in table 5.4 and hence share the same color.

Mode j	GR $\lvert\tilde{\lambda}_j\rvert$	Freq. (Hz) $\mathrm{Im}[\ln\tilde{\lambda}_j]/(2\pi T_s)$	Norm $\lVert\tilde{\boldsymbol{v}}_j\rVert$
1	1.0000	0	$3.9 \cdot 10^5$
2	0.9987	1.04	0.0629
3	0.9983	1.72	0.2194
4	0.9983	0	$5.6 \cdot 10^5$
5	0.9982	3.36	0.0024
6	0.9979	4.82	0.0001
7	0.9975	4.46	0.0027
8	0.9973	2.60	0.0265
9	0.9969	2.26	0.0059
10	0.9967	0.66	0.0546

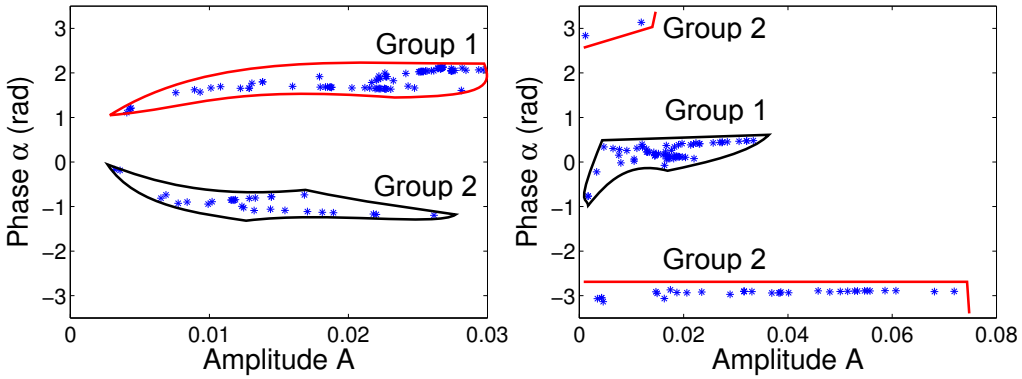

(a) Coherency, Mode 2 (1.04 Hz) (b) Coherency, Mode 3 (1.72 Hz)

Figure 5.13: Phase vs. amplitude plots for (a) Mode 2 (1.04 Hz) and (b) Mode 3 (1.72 Hz).

neighboring buses. The associated partitions are shown in figure 5.14.

As shown above, each dominant oscillatory KM provides a partition of the power grid. That is, the proposed method provides a set of partitions based on multiple frequencies. The variety of partitions possibly enhances the performance of the controlled islanding strategy: see [41].

The results of grid partitioning based on KMA and spectral graph theory were considered earlier. Now, a relationship between the theories is demonstrated by using data on dynamics of the test system according to ***Case 2***. Figure 5.15 depicts the oscillatory response of the bus voltage angles according to ***Case 2***. $N+1 = 541$ samples are acquired with $f_s = 60$ Hz and 540 KMs are obtained. Then, the second

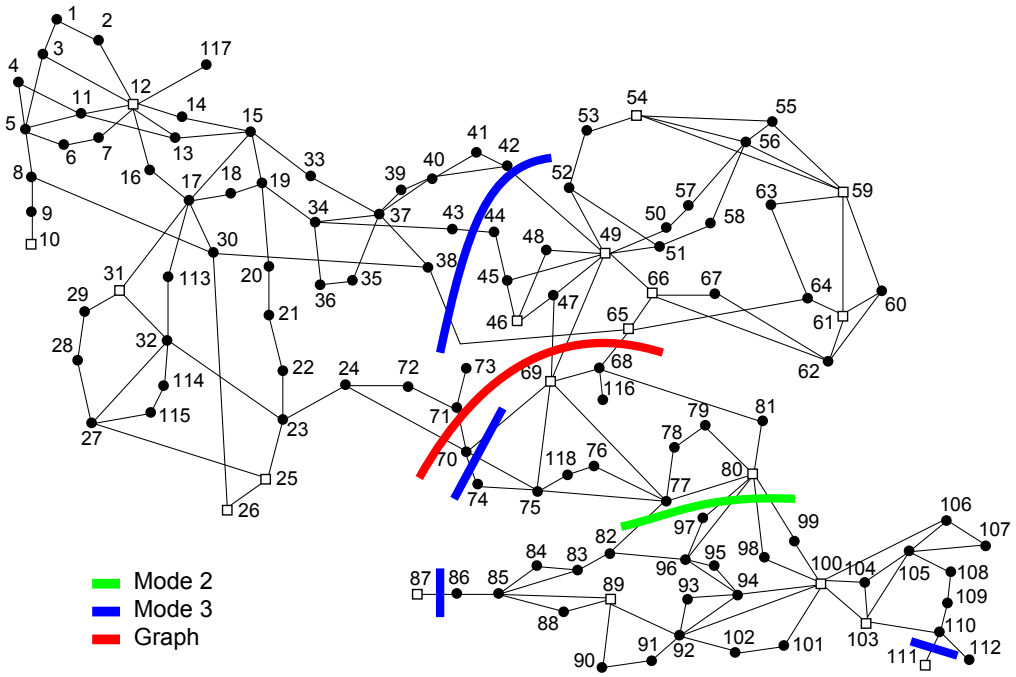

Figure 5.14: Partitioning of the IEEE 118-bus test system according to Mode 2, Mode 3 and spectral graph theory. The cut-sets are indicated by colored lines.

0 Hz mode, $\tilde{\boldsymbol{v}}_{\mathrm{NO2}}$ is identified among the KMs, a mode in which all components are real valued. In figure 5.16(a), $\tilde{\boldsymbol{v}}_{\mathrm{NO2}}$ is plotted against bus numbers. A similar plot can be observed for $\mathbf{V}_2$ in figure 5.16(b). The correlation coefficient of the two data sets is calculated in MATLAB according to

$$R = \frac{C(i,j)}{\sqrt{C(i,i)C(j,j)}}, \tag{5.2}$$

where $C(i,j)$ is the covariance between i and j. $R = 0.89$ is obtained and hence the data sets have a strong correlation. The reason for this is explained in section 5.4.

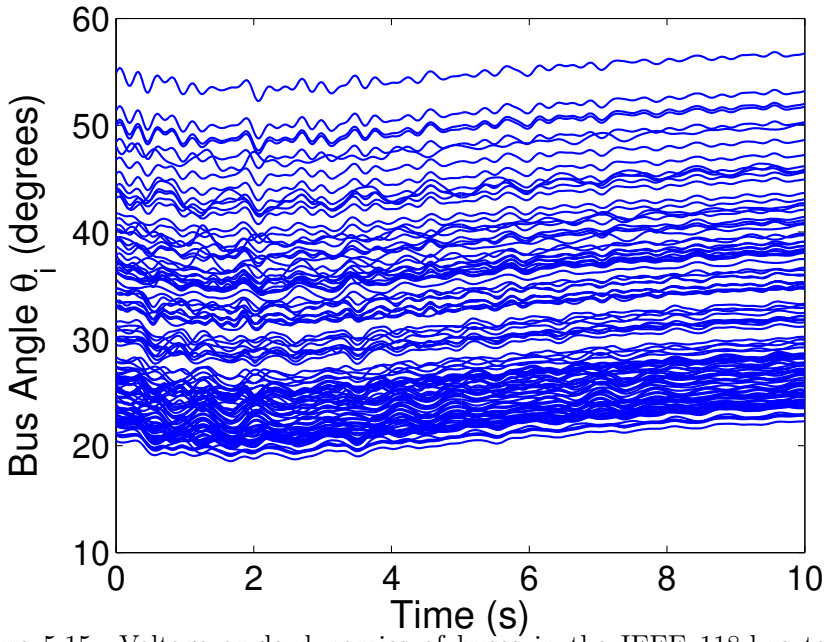

Figure 5.15: Voltage angle dynamics of buses in the IEEE 118-bus test system following disturbance of initial rotor frequencies according to ***Case 2***.

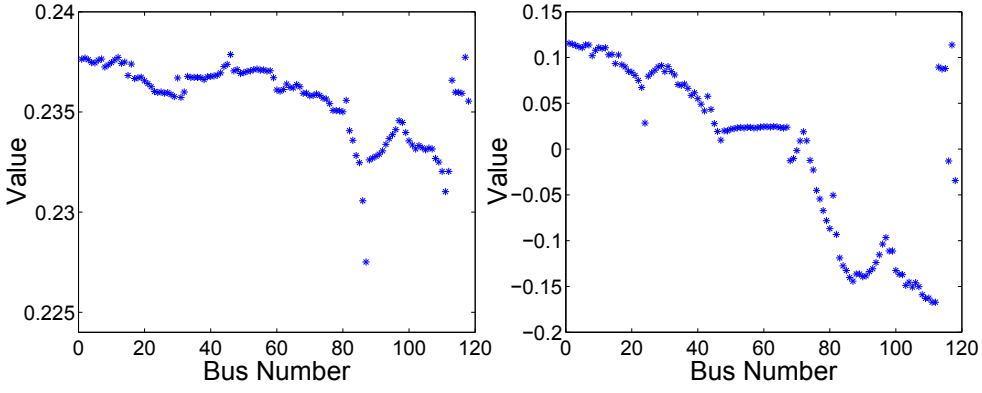

(a) $\tilde{\boldsymbol{v}}_{\mathrm{NO2}}$ (b) $\mathbf{V}_2$

Figure 5.16: (a) $\tilde{\boldsymbol{v}}_{\mathrm{NO2}}$ for the ***Case 2*** disturbance and (b) graph Laplacian's second eigenvector $\mathbf{V}_2$ plotted against bus numbers.

5.3.3 Time-Domain Simulations of Grid Splitting

For the ***Case 1*** fault, t_{cc} becomes approximately 360 ms. For a $t_c > t_{cc}$ instability occurs instantaneously and PSAT terminates. Thus, t_c is set to 350 ms, slightly below t_{cc} and the performance of the splitting is investigated with this setting.

The grid is now separated according to the partitions obtained from the two dominant modes (Mode 2 and 3), the fine partition and partition obtained from spectral graph theory. The data for the cut-sets are given in table 5.6 including tie-lines, generator groups and the factor $\Delta P/G_{tot}$ indicating the load-generation imbalance caused by the splitting.

For all the responses shown in figures 5.17(a)-5.17(d), synchronism is maintained between generators after the separation. The difference between the cases are the frequency deviation from steady state (1 p.u.). In table 5.6 the factor $\Delta P/G_{tot}$ indicates the load-generation discrepancy for each island formed.

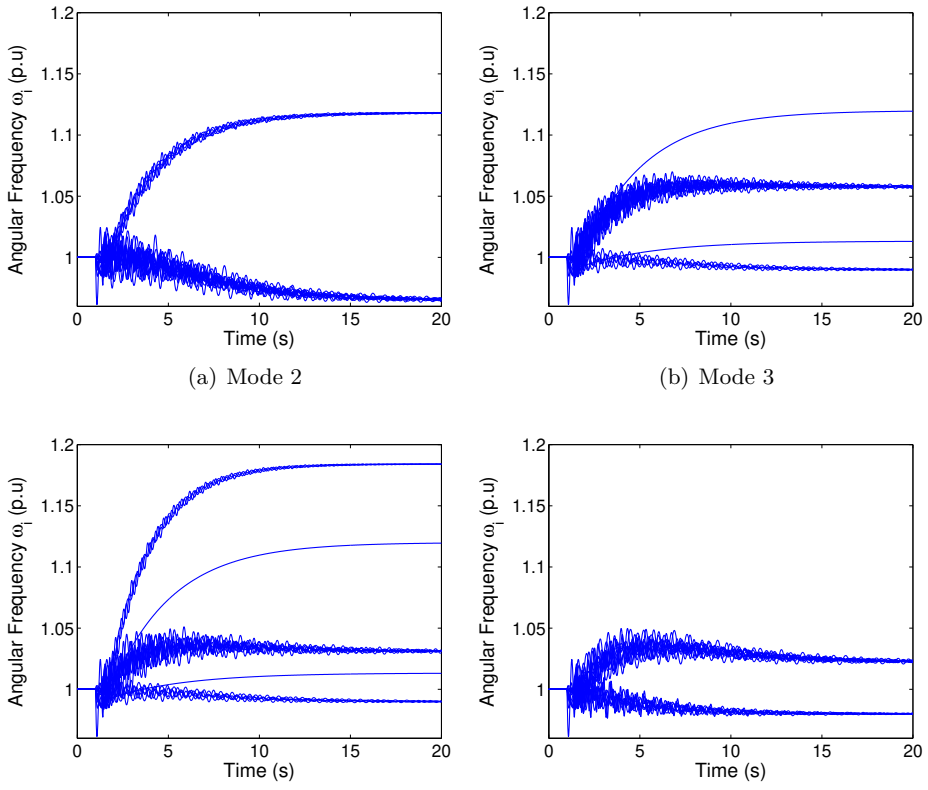

(a) Mode 2

(b) Mode 3

(c) Fine Partition

(d) Graph Theory

Figure 5.17: The four partitions are investigated during the event of a large fault and the test system is split according to (a) Mode 2, (b) Mode 3, (c) fine partition and (d) spectral graph theory.

Table 5.6: The data of the cut-sets illustrated in figure 5.14. The tie-lines are the lines connecting two groups of buses and a line is denoted in the table as $(b_{\text{fr}}, b_{\text{to}})$, where b_{fr} is the *from-bus* and b_{to} is the *to-bus*. $\Delta P_{\text{X}\to\text{Y}}$ is the power mismatch in Group X caused by disconnecting the tie-lines from Group X (Gr. X) to group Y where a positive sign (+) implies that power are being exported from Gr. X to Gr. Y. $\Delta P/G_{\text{tot}}$ is the power mismatch divided by the sum of the real power output of the generators in the group.

Cut-set	Tie-lines $(b_{\text{fr}}, b_{\text{to}})$	Generators	$\Delta P/G_{\text{tot}}$
Mode 2	(77,82), (80,96), (80,97), (80,98), (80,99)	**Gr. 1:** {10,12,25,26, 31,46,49,54,59,61,65, 66,69,80} **Gr. 2:** {87,89,100,103,111}	**Gr. 1:** $\Delta P_{1\to2} = 1.06$ $\Delta P_{1\to2}/G_{\text{tot1}} = -4.33$ % **Gr. 2:** $\Delta P_{2\to1} = -1.06$ $\Delta P_{2\to1}/G_{\text{tot2}} = -7.85$ %
Mode 3	(43,44), (42,49), (42,49), (38,65), (69,70), (70,74), (70,75), (86,87), (110,111)	**Gr. 1:** {10,12,25,26,31} **Gr. 2:** {46,49,54,59, 61,65,66,69,80. 89,100,103} **Gr. 3:** {87} **Gr. 4:** {111}	**Gr. 1:** $\Delta P_{1\to2} = -2.29$ $\Delta P_{1\to2}/G_{\text{tot1}} = -21.3$ % **Gr. 2:** $\Delta P_{2\to1,3,4} = 1.89$ $\Delta P_{2\to1,3,4}/G_{\text{tot2}} = 7.06$ % **Gr. 3:** $\Delta P_{3\to2} = 0.04$ $\Delta P_{3\to2}/G_{\text{tot3}} = 98.5$ % **Gr. 4:** $\Delta P_{4\to2} = 0.36$ $\Delta P_{4\to2}/G_{\text{tot4}} = 99$ %
Fine Part.	Mode 2 & 3's tie-lines	**Gr. 1:** {10,12,25,26,31} **Gr. 2:** {46,49,54,59, 61,65,66,69,80} **Gr. 3:** {89,100,103} **Gr. 4:** {87} **Gr. 5:** {111}	**Gr. 1:** $\Delta P_{1\to2,3} = -2.29$ $\Delta P_{1\to2,3}/G_{\text{tot1}} = -21.3$ % **Gr. 2:** $\Delta P_{2\to1,3} = 1.53$ $\Delta P_{2\to1,3}/G_{\text{tot2}} = +11.7$ % **Gr. 3:** $\Delta P_{3\to2,4,5} = 0.66$ $\Delta P_{3\to2,4,5}/G_{\text{tot3}} = +7.37$ % **Gr. 4:** $\Delta P_{4\to3} = 0.04$ $\Delta P_{4\to3}/G_{\text{tot4}} = 98.5$ % **Gr. 5:** $\Delta P_{5\to3} = 0.36$ $\Delta P_{5\to3}/G_{\text{tot5}} = 99$ %

Graph Th.	(65,68), (47,69), (49,69), (24,70), (70,71)	**Gr. 1:** {10,12,25,26, 31,46,49,54,59,61,65 66} **Gr. 2:** {69,80,87,89, 100,103,111}	**Gr. 1:** $\Delta P_{1\to 2} = 0.85$ $\Delta P_{1\to 2}/G_{\text{tot1}} = +3.47$ % **Gr. 2:** $\Delta P_{2\to 1} = -0.85$ $\Delta P_{2\to 1}/G_{\text{tot2}} = -6.29$ %

5.4 Discussion

5.4.1 Islanding Performance Factors

According to the literature study and the results obtained for the two test systems, three important factors governing the performance of a controlled islanding strategy were identified in the previous sections:

1. Synchronism between generators.
2. Load-generation balance within the islands.
3. Timing of grid-splitting.

The timing of the power grid splitting was a disregarded factor in this investigation as previously mentioned (see simulation setting in section 5.1.2). Nonetheless, a shorter or longer delay of the splitting affects the performance drastically for any of the cut-sets investigated. However, it is shown that KMA-monitoring of dynamics enables detection of disturbances and instabilities, see figure B.1. In the following, let us discuss the other two factors (1-2) with respect to the results obtained.

5.4.2 IEEE 68-Bus Test System

For the IEEE 68-bus system, the islanding performance was investigated for a critical disturbance, i.e. instability occurs within seconds after the clearing of the fault if no control measures are taken. With a controlled islanding operation for the four sets of tie-lines presented in table 5.3, the performance was improved in the sense that for the cases in which instability occurred anyway (shown in figures 5.9(a)-5.9(c)), an instability phenomena was delayed. For the Mode 3 partition (figure 5.9(a)), the splitting caused an instantaneous loss of synchronism between the generators. For the Mode 6 partition (figure 5.9(b)), the splitting itself did not cause any immediate loss of synchronism, but one generator diverges ≈ 10 s into the post-fault dynamics. The combination of Mode 3 and 6 (the fine partition) maintained generators in synchronism for a longer period of time ≈ 15 s. The idea of the fine partition was to provide partitions *multiple coherent* for two or more dominant modes (frequencies) and thus this result was not unexpected.

The partition obtained from spectral graph theory separated the test system into two parts. Following the splitting, instability was avoided and the two sub-grids converged with two separate frequencies. One group with a surplus of power generation and consequently left the other one with a deficiency. The same cut-set was included in the partitioning according to Mode 3, see figure 5.7.

The NETS-NYPS partition (captured by graph theory and Mode 3) provided the best result in terms of least amount of tie-lines disconnected and the best load-generation imbalance compared to the other partitions. Also, this was the only cut-set with maintained synchronism between generators upon separation.

5.4.3 IEEE 118-Bus Test System

The IEEE 118-bus system was simulated with a three-phase fault disturbance with a clearing time t_c just below critical clearing time t_{cc}. For all four cases of partitions, generators kept synchronism within the groups in the post-splitting dynamics. The KMA did not exactly capture the graph theoretic partition for the ***Case 1*** fault-case. However, interestingly, for a generator frequency displacement for all generators inducing oscillations close to the steady state (***Case 2*** disturbance), the connectivity measurement from spectral graph theory was identified with the KMA.

5.4.4 Koopman Modes and Spectral Graph Theory

It was shown in section 5.3.2 that a strong correlation existed between a certain KM (denoted as the second 0 Hz mode, $\tilde{\boldsymbol{v}}_{\mathrm{NO2}}$) and the second eigenvector for the graph Laplacian (a measurement of connectivity). Now the correlation is theoretically explained, in other words, why the spectral graph connectivity is captured using the KMA on dynamics. First of all, by applying the ***Case 2*** disturbance, a response exhibiting dynamics close to the initial operating point is achieved. In PSAT the dynamics are calculated from a set of nonlinear differential-algebraic equations:

$$\begin{aligned} \frac{d\boldsymbol{x}}{dt} &= \boldsymbol{f}(\boldsymbol{x}, \boldsymbol{y}), \\ \mathbf{0} &= \boldsymbol{g}(\boldsymbol{x}, \boldsymbol{y}), \end{aligned} \tag{5.3}$$

where $\boldsymbol{x} = (\delta_1, \ldots, \delta_{19}, \omega_1, \ldots, \omega_{19})^{\mathrm{T}}$ is the set of state variables and $\boldsymbol{y}$ is the set of output variables consisting of bus voltages $\boldsymbol{v} = (v_1, \ldots, v_{118})^{\mathrm{T}}$ and bus voltage angles $\boldsymbol{\theta} = (\theta_1, \ldots, \theta_{118})^{\mathrm{T}}$. Here the vector-valued function $\boldsymbol{g}$ represents the power flow equations of the grid and is decomposed in [40] as follows:

$$\begin{aligned} \mathbf{0} &= \boldsymbol{g_1}(\boldsymbol{x}, \boldsymbol{v}, \boldsymbol{\theta}), \\ \mathbf{0} &= \boldsymbol{g_2}(\boldsymbol{x}, \boldsymbol{v}, \boldsymbol{\theta}), \end{aligned} \tag{5.4}$$

where $\boldsymbol{g}_1$ describes the reactive power flows and $\boldsymbol{g}_2$ the active power flows. Under the singular perturbation theory [42], $\boldsymbol{x}$ describes the slow dynamics of the grid, and $\boldsymbol{y}$ its fast dynamics. According to the standard scaling argument (see [42]), the so-called boundary layer system exhibiting the fast dynamics of the grid is derived as follows:

$$\begin{aligned} \frac{d\boldsymbol{x}}{d\tau} &= \mathbf{0}, \\ \frac{d\boldsymbol{v}}{d\tau} &= \boldsymbol{g_1}(\boldsymbol{x}, \boldsymbol{v}, \boldsymbol{\theta}), \\ \frac{d\boldsymbol{\theta}}{d\tau} &= \boldsymbol{g_2}(\boldsymbol{x}, \boldsymbol{v}, \boldsymbol{\theta}), \end{aligned} \tag{5.5}$$

where τ is a new time variable. Now, because the short-term electro-mechanical dynamics close to the initial steady state is analyzed, bus voltages $\boldsymbol{v}$ are assumed to

be constant, and the differences of bus angles between any two buses are assumed small. Thus, by recalling that the active power flows are represented by $\boldsymbol{g_2}$, (5.5) is rewritten as

$$\begin{aligned} \frac{d\boldsymbol{\theta}}{d\tau} &= \boldsymbol{g_2}(\boldsymbol{x}_{\mathrm{Q}}, \boldsymbol{v}_{\mathrm{Q}}, \boldsymbol{\theta}_{\mathrm{Q}}) + (\mathrm{D}_{\theta}\boldsymbol{g}_2)(\boldsymbol{x}_{\mathrm{Q}}, \boldsymbol{v}_{\mathrm{Q}}, \boldsymbol{\theta}_{\mathrm{Q}})\boldsymbol{\theta} + \text{h.o.t.}, \\ &\approx \boldsymbol{g_2}(\boldsymbol{x}_{\mathrm{Q}}, \boldsymbol{v}_{\mathrm{Q}}, \boldsymbol{\theta}_{\mathrm{Q}}) + \mathsf{L}_{\mathrm{W}}\boldsymbol{\theta}, \end{aligned} \tag{5.6}$$

where $(\boldsymbol{x}_{\mathrm{Q}}, \boldsymbol{v}_{\mathrm{Q}}, \boldsymbol{\theta}_{\mathrm{Q}})$ denotes the initial steady state, and L_{W} corresponds to the Laplacian matrix weighted by positive constants $v_i v_j B_{ij}$ (B_{ij} is the susceptance of the line between buses i and j). That is, the linearized bus dynamics are represented by the positively-weighted Laplacian matrix of the grid. This is why the KMA of bus angle dynamics close to the initial steady state captures well the intrinsic graph-structural properties of the grid.

The second 0 Hz mode ($\tilde{\boldsymbol{v}}_{\mathrm{NO2}}$), is not only identified for the IEEE 118-bus test system. For the 68-bus test case, a similar result is also obtained. Depending on the disturbance and also the sampling duration, the connectivity property of spectral graph theory is obtained with stronger or weaker correlation.

Chapter 6

Closure

6.1 Summary

This thesis investigates the possibilities of a new power grid islanding strategy based on the Koopman Mode Analysis (KMA). By measuring voltage angle dynamics of every bus in two test systems, partitions are determined for dominant modes. The dynamics of the response are decomposed into a finite number of modes (each with a frequency) using KMA. A dominant mode corresponds to a predominant frequency identified in the dynamics following a fault in the system.

In graph theory, a power grid is represented by vertices (buses or nodes) and edges connecting the vertices (transmission lines). By investigating the matrix properties of the power grid representation, a connectivity property is achieved. On the other hand, the measurements of voltage angle dynamics provides the nodal or vertex dynamics of a graph. It is shown in this thesis that the connectivity property obtained from spectral graph theory could be verified by KMA on nodal dynamics, with a strong correlation.

Simulations showed that the partitions obtained from KMA and spectral graph theory could indeed improve the performance following a severe fault. However, a vital step in a controlled islanding strategy is to determine which one out of several cut-sets that are most suitable for the islanding. This is not yet clarified for the KMA-based controlled islanding strategy.

6.2 Conclusions and Contributions

The contributions of this thesis are two-fold. First, the thesis provides a new method of partitioning power grids based on the nonlinear KMA. By applying the method to the IEEE 118 and 68 test systems, it was demonstrated that the KMA provides cut-sets splitting the test systems into isolated sub-grids. This leads to the KMA-based controlled islanding strategy.

Second, it is shown that the KMA also captures characteristics described by spectral graph theory, particularly for dynamics exhibiting oscillations close to the

steady state which was shown for the IEEE 118-bus test system. For the IEEE 68-bus test system, the cut-set from graph theory was even directly obtained from one of the dominant oscillatory modes for a large fault.

In the case of cascading dynamics in a real power grid far from steady state conditions, a method which can fully capture and provide partitions with respect to the complex nonlinear dynamics should be considered. Thus, the KMA is regarded as a powerful prospect in monitoring and control of complex power grids.

The development of new sophisticated strategies for protecting and maintaining the safe operation of vital systems like power grids are important for the society. It is also and one of the pieces in the puzzle for the next generation power grids called *smart grids*. Almost every vital function in the society today depends on the stable supply of electricity and the development of the new power grid gives economical, environmental and safety gains.

6.3 Future Studies

There are several future studies required to establish a complete and sophisticated controlled islanding strategy based on the KMA. The two most important steps are listed below.

1. Determine the best cut-set from a selection of possible cut-sets.
2. Determine an optimal separation timing for the cut-set.

Determining a best cut-set from a set of possible cut-sets is a vital part of the controlled islanding strategy. This could be done in two steps. First, impose constraints such as a minimum load-generation imbalance. Second, for every sub-grid, a pre-assessment of the stability is conducted. Previously, a pre-assessment of islanding stability has been conducted in [43].

The separation timing is a complicated task. Firstly, an emergency situation has to be detected by the monitoring system. Depending on the type and location of the disturbance it could be beneficial to split as soon as possible or delay the splitting for a certain amount of time. For example, the time duration from a stable state to a blackout state can range from seconds to minutes. It is possible that the islanding operation causes even more turbulence and failure in the system if split incorrectly or with an inappropriate timing. It is shown in figure B.1 in the appendix, that monitoring dynamics with KMA on a short time-scale enables detection of disturbances and instabilities. More investigation on KMA-monitoring and how this can trigger an islanding operation is an interesting future subject of research.

Appendix A

Power System Analysis

In the following a short theoretical description of the mathematics simulated in the test cases are given, see [40, 44] for details.

A.1 System Equations and Modeling

The most simple representation of a generator used in transient studies is the classical model shown in figure A.1. The classical model is used for the IEEE 118-bus test case in section 5.3. The generator is described by a constant voltage $\bar{E}^{'}$ $(= E^{'}\angle\delta)$ behind its transient reactance $X_d^{'}$. The voltage at the generator bus is denoted as $\bar{v}$ $(=v\angle\theta)$.

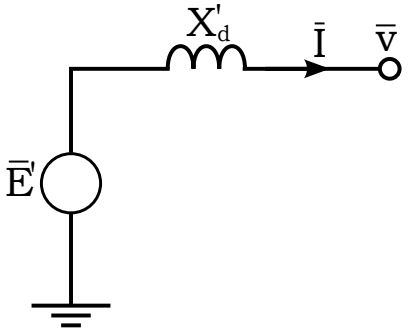

Figure A.1: Classical model of a synchronous generator for transient studies.

The injected real power P_e delivered to the k-th bus by its associated generator is given by

$$P_e = \frac{E_k^{'} v_k}{x_d^{'}} \sin(\delta_k - \theta_k). \tag{A.1}$$

The dynamics of the generators are described by the following two differential equations:

$$\begin{aligned} \dot{\delta}_k &= \omega_k, \\ \dot{\omega}_k &= \frac{1}{M_k}\left(P_{mk} - P_e - D\omega_k\right), \end{aligned} \tag{A.2}$$

where δ is the rotor angle, ω the rotor frequency deviation from equilibrium point and D the damping. M_k is given by

$$M_k = \frac{2HS_k^b}{\omega_s S_b^{3\phi}}, \tag{A.3}$$

where H is the generator's inertia constant ($\approx$ a few seconds), ω_s is the system synchronous speed ($2\pi f_s$), $S_b^{3\phi}$ is the rated three-phase power for the system and S_k^b is the generator's rated power. For the IEEE 68-bus test case in section 5.2, a generator model in which generator voltages are not constant is used (see PSAT manual, generator model IV and Automatic Voltage Regulator (AVR) type II).

The injected active and reactive powers for every bus k bus are given by the following nonlinear algebraic equations:

$$\begin{aligned} P_k &= v_k \sum_{m=1}^{n} \left(G_{km} v_m \cos\theta_{km} + B_{km} v_m \sin\theta_{km}\right) + P_e, \\ Q_k &= v_k \sum_{m=1}^{n} \left(G_{km} v_m \sin\theta_{km} - B_{km} v_m \cos\theta_{km}\right) + P_e, \end{aligned} \tag{A.4}$$

where $P_e = 0$ for non-generator buses and G_{km} and B_{km} is the conductance and susceptance in the admittance matrix Y between bus k and m respectively, see [40] for further explanations. In every bus, there is a balance between injected and consumed active and reactive power given by:

$$\begin{aligned} 0 &= P_k + P_{Lk}, \\ 0 &= Q_k + Q_{Lk}, \end{aligned} \tag{A.5}$$

where P_{Lk} and Q_{Lk} is the active and reactive load at bus k, respectively. The set of nonlinear differential and algebraic equations is denoted as

$$\begin{aligned} \dot{\boldsymbol{x}} &= \boldsymbol{f}(\boldsymbol{x}, \boldsymbol{y}), \\ \boldsymbol{0} &= \boldsymbol{g}(\boldsymbol{x}, \boldsymbol{y}), \end{aligned} \tag{A.6}$$

where $\boldsymbol{f}$ is the set of differential equations governing the generator dynamics and $\boldsymbol{g}$ is the set of algebraic equations maintaining the power balance for buses. $\boldsymbol{x} = (\delta_1, \ldots, \delta_{19}, \omega_1, \ldots, \omega_{19})^{\mathrm{T}}$ is the set of state variables and $\boldsymbol{y}$ is the set of output variables consisting of bus voltages $\boldsymbol{v} = (v_1, \ldots, v_{118})^{\mathrm{T}}$ and bus voltage angles $\boldsymbol{\theta} = (\theta_1, \ldots, \theta_{118})^{\mathrm{T}}$. The dynamics are simulated using the Power System Analysis Toolbox (PSAT) [10], which is an open source toolbox for MATLAB.

A.2 Center of Inertia

It is common to transform (A.6) into the so-called Center Of Inertia (COI) reference frame. COI is a point in the system defined by the following set of equations.

$$\delta_{COI} = \frac{1}{M_T}\sum_{k=1}^{n} M_k\delta_k, \quad \omega_{COI} = \frac{1}{M_T}\sum_{k=1}^{n} M_k\omega_k, \quad M_T = \sum_{k=1}^{n} M_k. \tag{A.7}$$

The measured observables such as rotor angles δ, generator angular frequencies ω and bus voltage angles θ are expressed in the COI reference frame as follows.

$$\tilde{\delta}_{COI} = \delta_k - \delta_{COI}, \qquad \tilde{\omega}_{COI} = \omega_k - \omega_{COI}, \qquad \tilde{\theta}_{COI} = \theta_k - \delta_{COI}. \tag{A.8}$$

See [44] for more information.

A.3 Small Signal Analysis - Modal Analysis

The linearization of (A.6) around its equilibrium point is expressed as following:

$$\begin{aligned} \Delta\dot{\boldsymbol{x}} &= \boldsymbol{f_x}\Delta\boldsymbol{x} + \boldsymbol{f_y}\Delta\boldsymbol{y}, \\ \mathbf{0} &= \boldsymbol{g_x}\Delta\boldsymbol{x} + \boldsymbol{g_y}\Delta\boldsymbol{y}, \end{aligned} \tag{A.9}$$

where

$$\begin{aligned} \boldsymbol{f}_x &= \left[\frac{\partial \boldsymbol{f}(x_0, y_0)}{\partial x}\right], \qquad \boldsymbol{f}_y = \left[\frac{\partial \boldsymbol{f}(x_0, y_0)}{\partial y}\right], \\ \boldsymbol{g}_x &= \left[\frac{\partial \boldsymbol{g}(x_0, y_0)}{\partial x}\right], \qquad \boldsymbol{g}_y = \left[\frac{\partial \boldsymbol{g}(x_0, y_0)}{\partial y}\right], \end{aligned} \tag{A.10}$$

where $\boldsymbol{f}$ is the set of differential equations describing generator dynamics (see (A.2) for classical model) and $\boldsymbol{g}$ is represented by the set of equations (A.2)-(A.4). Now, (A.9) can be re-written as

$$\Delta\dot{\boldsymbol{x}} = (\boldsymbol{f}_x - \boldsymbol{f}_y\left(\boldsymbol{g}_y\right)^{-1}\boldsymbol{g}_x)\Delta\boldsymbol{x} = \mathrm{A}\Delta\boldsymbol{x}, \tag{A.11}$$

and the eigenvalues are given by

$$\det\left(\mathrm{A} - \lambda\mathbb{1}\right) = 0, \tag{A.12}$$

where the damping ξ_j for each mode (eigenvalue) $\lambda_j = \sigma_j \pm j\omega_j$ is given by

$$\xi_j = \frac{-\sigma_j}{\sqrt{\sigma_j^2 + \omega_j^2}}, \tag{A.13}$$

and the frequency f_j is calculated as

$$f_j = \frac{\omega_j}{2\pi}. \tag{A.14}$$

Appendix B

Short-Time Koopman Mode Monitoring

Here, let us now apply the KMA to the unstable fault case shown in figure B.1(a). In the KMA-partitioning in section 5.2.2, KMs were calculated based on a large number of samples (541). Here, let us investigate the KMs calculated based on fewer samples (30) which corresponds to 0.5 s ($f_s = 60$ Hz) of sampled dynamics. Multiple sets of KMs are calculated. Two consecutive sets of KMs have an overlap of 24 samples. The result is shown in figure B.1(b) and can be regarded as a KM *spectrogram*. In the figure, the frequency associated for every mode is shown as constant for the time period it is calculated for (0.5 s) and colored from red (large Growth Rate (GR)) to blue (small GR). By inspecting the spectrogram, a clear and sudden increase in GR is visible just prior to the loss of synchronism between the two groups of generators. By monitoring dynamics in this manner, it is possible to detect instabilities and trigger an islanding operation of a grid.

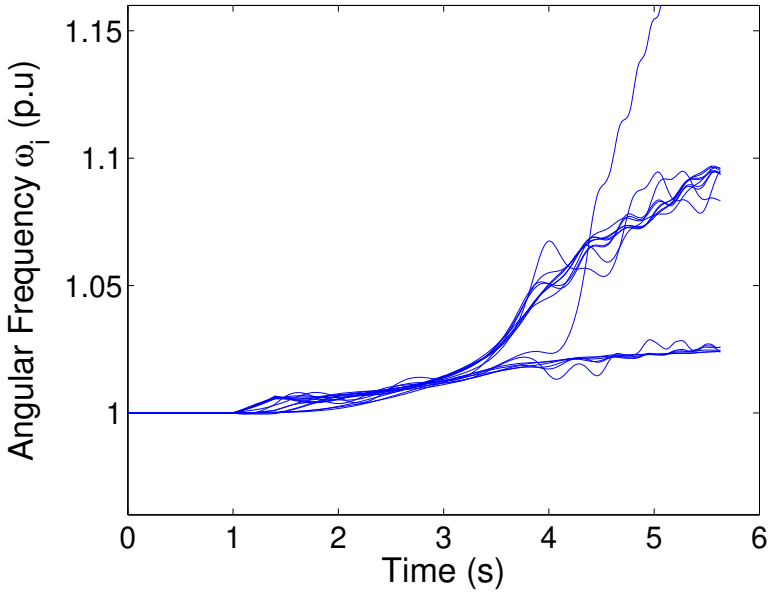

(a) Unstable fault

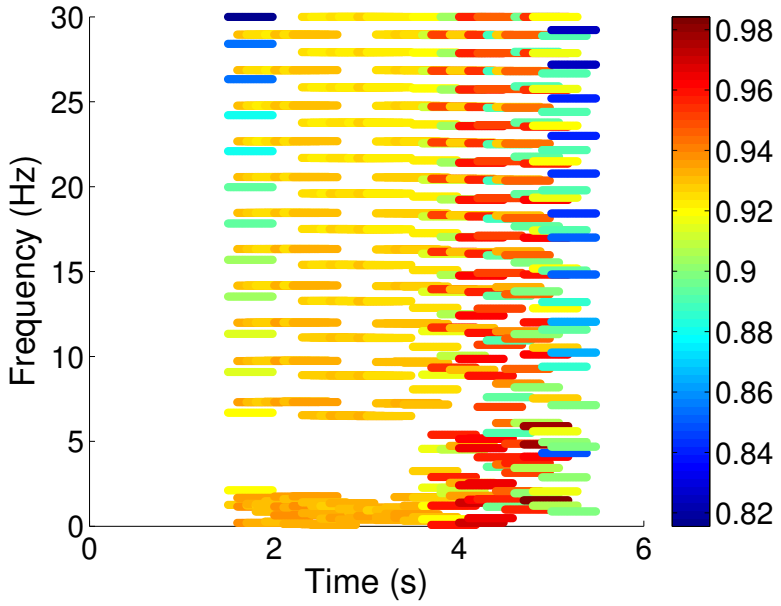

(b) Short-time Koopman modes

Figure B.1: (a) Angular frequency response of generators for an unstable fault and (b) short-time (0.5 s) Koopman mode frequencies calculated for the response. Every modal frequency is colored based on the growth rate.

Appendix C

Submitted Reports and Papers

One technical report and one conference paper were written and submitted during the project and they are briefly described below.

(i) F. Raak, Y. Susuki, T. Hikihara, and H. Chamorro, "Investigation of power grid islanding based on nonlinear Koopman modes," in *IEICE Technical Report, Nonlinear Problems*, vol. 113, pp. 75–80, 2013

A technical report was submitted to the IEICE Technical Meeting on Nonlinear Problems (NLP) with the title "Investigation of Power Grid Islanding Based on Nonlinear Koopman Modes" [41]. The meeting was held in Miyakojima (Japan) in July 2013. The report describes how a power grid can be separated in two or several sub-grids by means of the KMA. The proposed separation method was compared to another method based on spectral graph theory. It was shown in this report that the result from spectral graph theory was also captured by the KMA-based method.

(ii) F. Raak, Y. Susuki, T. Hikihara, H. Chamorro, and M. Ghandhari, "Partitioning power grids via nonlinear Koopman mode analysis," in *IEEE PES Conference on Innovative Smart Grid Technologies, ISGT Washington*, 2014. (Submitted)

A paper [45] was submitted to The Innovative Smart Grid Technologies (ISGT) conference in Washington DC (US) which will be held in February 2014. Similar to the technical report, it demonstrates the ability to identify separation boundaries in a power grid using the KMA-based method on sampled dynamics. More than that, it is shown that KMA indeed captures the intrinsic structural properties of the spectral graph theory which was first suspected in the IEICE Technical Meeting report.

Bibliography

[1] B. A. Carreras, V. E. Lynch, I. Dobson, and D. E. Newman, "Complex dynamics of blackouts in power transmission systems," *Chaos*, vol. 14, no. 3, pp. 643–652, 2004.

[2] G. Andersson, P. Donalek, R. Farmer, N. Hatziargyriou, I. Kamwa, P. Kundur, N. Martins, J. Paserba, P. Pourbeik, J. Sanchez-Gasca, R. Schulz, A. Stankovic, C. Taylor, and V. Vittal, "Causes of the 2003 major grid blackouts in North America, Europe, and recommended means to improve system dynamic performance," *IEEE Transactions on Power Systems*, vol. 20, no. 4, pp. 1922–1928, 2005.

[3] J. Romero, "Blackouts illuminate India's power problems," *Spectrum, IEEE*, vol. 49, no. 10, pp. 11–12, 2012.

[4] S. Corsi and C. Sabelli, "General blackout in Italy sunday September 28, 2003, h. 03:28:00," in *2004 IEEE Power Engineering Society General Meeting*, vol. 2, pp. 1691–1701, 2004.

[5] I. Mezić, "Spectral properties of dynamical systems, model reduction and decompositions," *Nonlinear Dynamics*, vol. 41, no. 1-3, pp. 309–325, 2005.

[6] C. W. Rowley, I. Mezić, S. Bagheri, P. Schlatter, and D. S. Henningson, "Spectral analysis of nonlinear flows," *Journal of Fluid Mechanics*, vol. 641, pp. 115–127, 2009.

[7] Y. Susuki and I. Mezić, "Nonlinear Koopman modes and coherency identification of coupled swing dynamics," *IEEE Transactions on Power Systems*, vol. 26, no. 4, pp. 1894–1904, 2011.

[8] Y. Susuki and I. Mezić, "Nonlinear Koopman modes and a precursor to power system swing instabilities," *IEEE Transactions on Power Systems*, vol. 27, no. 3, pp. 1182–1191, 2012.

[9] Y. Susuki and I. Mezić, "Nonlinear Koopman modes and power system stability assessment without models," *IEEE Transactions on Power Systems*, 2013. (In revision).

[10] F. Milano, "An open source power system analysis toolbox," *IEEE Transactions on Power Systems*, vol. 20, no. 3, pp. 1199–1206, 2005.

[11] Y. V. Makarov, V. I. Reshetov, V. A. Stroev, and N. I. Voropai, "Blackout prevention in the United States, Europe, and Russia," *Proceedings of the IEEE*, vol. 93, no. 11, pp. 1942–1954, 2005.

[12] P. Fairley, "The unruly power grid," *IEEE Spectrum*, vol. 41, no. 8, pp. 16–21, 2004.

[13] J. De La Ree, V. Centeno, J. S. Thorp, and A. G. Phadke, "Synchronized phasor measurement applications in power systems," *IEEE Transactions on Smart Grid*, vol. 1, no. 1, pp. 20–27, 2010.

[14] R. Albert, I. Albert, and G. L. Nakarado, "Structural vulnerability of the north american power grid," *Physical Review E - Statistical, Nonlinear, and Soft Matter Physics*, vol. 69, no. 2 2, pp. 025103–1–025103–4, 2004.

[15] S. V. Buldyrev, R. Parshani, G. Paul, H. E. Stanley, and S. Havlin, "Catastrophic cascade of failures in interdependent networks," *Nature*, vol. 464, no. 7291, pp. 1025–1028, 2010.

[16] D. H. Boteler, R. J. Pirjola, and H. Nevanlinna, "The effects of geomagnetic disturbances on electrical systems at the Earth's surface," *Advances in Space Research*, vol. 22, no. 1, pp. 17–27, 1998.

[17] P. Pourbeik, P. S. Kundur, and C. W. Taylor, "The anatomy of a power grid blackout," *IEEE Power and Energy Magazine*, vol. 4, no. 5, pp. 22–29, 2006.

[18] P. Kundur, J. Paserba, V. Ajjarapu, G. Andersson, A. Bose, C. Canizares, N. Hatziargyriou, D. Hill, A. Stankovic, C. Taylor, T. Van Cursem, and V. Vittal, "Definition and classification of power system stability," *IEEE Transactions on Power Systems*, vol. 19, no. 3, pp. 1387–1401, 2004.

[19] A. E. Motter, S. A. Myers, M. Anghel, and T. Nishikawa, "Spontaneous synchrony in power-grid networks," *Nature Physics*, vol. 9, no. 3, pp. 191–197, 2013.

[20] C. W. Taylor, D. C. Erickson, K. E. Martin, R. E. Wilson, and V. Venkatasubramanian, "WACS - Wide-area stability and voltage control system: R&D and online demonstration," *Proceedings of the IEEE*, vol. 93, no. 5, pp. 892–906, 2005.

[21] I. Kamwa, R. Grondin, and Y. Hébert, "Wide-area measurement based stabilizing control of large power systems - A decentralized/hierarchical approach," *IEEE Transactions on Power Systems*, vol. 16, no. 1, pp. 136–153, 2001.

[22] H. You, V. Vittal, and X. Wang, "Slow coherency-based islanding," *IEEE Transactions on Power Systems*, vol. 19, no. 1, pp. 483–491, 2004.

[23] B. Yang, V. Vittal, and G. T. Heydt, "Slow-coherency-based controlled islanding - A demonstration of the approach on the August 14, 2003 blackout scenario," *IEEE Transactions on Power Systems*, vol. 21, no. 4, pp. 1840–1847, 2006.

[24] X. Wang and V. Vittal, "System islanding using minimal cutsets with minimum net flow," in *2004 IEEE PES Power Systems Conference and Exposition*, vol. 1, pp. 379–384, 2004.

[25] K. Sun, K. Hur, and P. Zhang, "A new unified scheme for controlled power system separation using synchronized phasor measurements," *IEEE Transactions on Power Systems*, vol. 26, no. 3, pp. 1544–1554, 2011.

[26] K. Sun, D. . Zheng, and Q. Lu, "Splitting strategies for islanding operation of large-scale power systems using OBDD-based methods," *IEEE Transactions on Power Systems*, vol. 18, no. 2, pp. 912–923, 2003.

[27] K. Sun, D. . Zheng, and Q. Lu, "A simulation study of OBDD-based proper splitting strategies for power systems under consideration of transient stability," *IEEE Transactions on Power Systems*, vol. 20, no. 1, pp. 389–399, 2005.

[28] R. Moreno and A. Torres, "Security of the power system based on the separation into islands," in *2011 IEEE PES Conference on Innovative Smart Grid Technologies Latin America SGT LA 2011 - Conference Proceedings*, 2011.

[29] M. Budišić, R. Mohr, and I. Mezić, "Applied Koopmanism," *Chaos*, vol. 22, no. 4, 2012.

[30] M. Fiedler, "Algebraic connectivity of graphs," *Czechoslovak Mathematical Journal*, vol. 23, no. 98, pp. 298–305, 1973.

[31] M. Fiedler, "A property of eigenvectors of nonnegative symmetric matrices and its application to graph theory," *Czechoslovak Mathematical Journal*, vol. 25, pp. 619–633, 1975.

[32] C. Desoer and E. Kuh, *Basic circuit theory*. McGraw-Hill, 1969.

[33] M. R. Aghamohammadi and A. Shahmohammadi, "Intentional islanding using a new algorithm based on ant search mechanism," *International Journal of Electrical Power and Energy Systems*, vol. 35, no. 1, pp. 138–147, 2012.

[34] Power Systems Test Case Archive, College of Engineering, University of Washington, URL: `http://www.ee.washington.edu/research/pstca/`.

[35] G. Rogers, *Power System Oscillations*. Kluwer Academic, 2000.

[36] S. Koch, S. Chatzivasileiadis, M. Vrakopoulou, and G. Andersson, "Mitigation of cascading failures by real-time controlled islanding and graceful load shedding," in *2010 IREP Symposium - Bulk Power System Dynamics and Control - VIII, IREP2010*, 2010.

[37] K. Sun, D. . Zheng, and Q. Lu, "Searching for feasible splitting strategies of controlled system islanding," *IEE Proceedings: Generation, Transmission and Distribution*, vol. 153, no. 1, pp. 89–98, 2006.

[38] L. Ding and V. Terzija, "A new controlled islanding algorithm based on spectral clustering," in *DRPT 2011 - 2011 4th International Conference on Electric Utility Deregulation and Restructuring and Power Technologies*, pp. 337–342, 2011.

[39] "IEEE standard for synchrophasor measurements for power systems," *IEEE Std C37.118.1-2011 (Revision of IEEE Std C37.118-2005)*, pp. 1–61, 2011.

[40] P. Kundur, *Power System Stability and Control*. McGraw-Hill, 1994.

[41] F. Raak, Y. Susuki, T. Hikihara, and H. Chamorro, "Investigation of power grid islanding based on nonlinear Koopman modes," in *IEICE Technical Report, Nonlinear Problems*, vol. 113, pp. 75–80, 2013.

[42] H. Khalil, *Nonlinear Systems*. Prentice Hall, 1996.

[43] P. McNabb and J. Bialek, "A priori transient stability indicator of islanded power systems using extended equal area criterion," in *IEEE Power and Energy Society General Meeting*, 2012.

[44] M. Ghandhari, *Stability of Power Systems*. Electric Power Systems, Royal Institute of Technology, Stockholm, Sweden, 2011.

[45] F. Raak, Y. Susuki, T. Hikihara, H. Chamorro, and M. Ghandhari, "Partitioning power grids via nonlinear Koopman mode analysis," in *IEEE PES Conference on Innovative Smart Grid Technologies, ISGT Washington*, 2014. (Submitted).